

# Quantum effects in optomechanical systems

C. Genes<sup>a</sup>, A. Mari<sup>b</sup>, D. Vitali<sup>c</sup>, and P. Tombesi<sup>c</sup>

<sup>a</sup>*Institute for Theoretical Physics, University of Innsbruck, and Institute for Quantum Optics and Quantum Information, Austrian Academy of Sciences, Technikerstrasse 25, A-6020 Innsbruck, Austria*

<sup>b</sup>*Institute of Physics and Astronomy, University of Potsdam, 14476 Potsdam, Germany*

<sup>c</sup>*Dipartimento di Fisica, Università di Camerino, via Madonna delle Carceri, I-62032, Camerino (MC) Italy*

---

## Abstract

The search for experimental demonstrations of the quantum behavior of macroscopic mechanical resonators is a fastly growing field of investigation and recent results suggest that the generation of quantum states of resonators with a mass at the microgram scale is within reach. In this chapter we give an overview of two important topics within this research field: cooling to the motional ground state, and the generation of entanglement involving mechanical, optical and atomic degrees of freedom. We focus on optomechanical systems where the resonator is coupled to one or more driven cavity modes by the radiation pressure interaction. We show that robust stationary entanglement between the mechanical resonator and the output fields of the cavity can be generated, and that this entanglement can be transferred to atomic ensembles placed within the cavity. These results show that optomechanical devices are interesting candidates for the realization of quantum memories and interfaces for continuous variable quantum communication networks.

*Key words:* radiation pressure, optical cavities, micromechanical systems, optomechanical devices, ground state cooling, quantum entanglement, atomic ensembles

*PACS:* 03.67.Mn, 85.85.+j, 42.50.Wk, 42.50.Lc

## Contents

1	Introduction	2
2	Cavity optomechanics via radiation pressure	5
2.1	Langevin equations formalism	6
2.2	Stability analysis	9
2.3	Covariance matrix and logarithmic negativity	9
3	Ground state cooling	11

3.1	Feedback cooling	12
3.2	Back-action cooling	17
3.3	Readout of the mechanical resonator state	19
4	Entanglement generation with a single driven cavity mode	21
4.1	Intracavity optomechanical entanglement	22
4.2	Entanglement with output modes	23
4.3	Optical entanglement between sidebands	27
5	Entanglement generation with two driven cavity modes	29
5.1	Quantum Langevin equations and stability conditions	30
5.2	Entanglement of the output modes	33
6	Cavity-mediated atom-mirror stationary entanglement	38
7	Conclusions	42
8	Acknowledgements	43
	References	43

---

## 1 Introduction

Mechanical resonators at the micro- and nano-meter scale are widely employed for a large variety of applications, more commonly as sensors or actuators in integrated electrical, optical, and opto-electronical systems [1,2,3,4]. Modifications of the resonator motion can be detected with high sensitivity by looking at the radiation (or electric current) which interacted with the resonator. For example, small masses can be detected by measuring the frequency shift induced on the resonator, while tiny displacements (or weak forces inducing such displacements) can be measured by detecting the corresponding phase shift of the light interacting with it [2]. The resonators are always subject to thermal noise, which is due to the coupling with internal and/or external degrees of freedom and is one of the main factors limiting the sensitivity of these devices. However, due to the progress in nanofabrication techniques, the mechanical quality factor  $Q_m$  (which quantifies this undesired coupling to environmental degrees of freedom) is steadily improving, suggesting that in the near future these devices will reach the regime in which their sensitivity is limited by the ultimate quantum limits set by the Heisenberg principle. The importance of the limits imposed by quantum mechanics on the resonator motion was first pointed out by Braginsky and coworkers [5] in the completely different context of *massive* resonators employed in the detection of gravitational waves [6]. However, in recent years the quest for the experimental demonstration of genuine quantum states of macroscopic mechanical resonators has spread well beyond the gravitational wave physics community and has attracted a

wide interest. In fact, the detection of an unambiguous signature of the quantum behavior of a macroscopic oscillator, with a mass at least of the order of a microgram, would shed further light onto the quantum-classical boundary problem [7]. In fact, nothing in the principles of quantum mechanics prevents macroscopic systems to be prepared in genuine quantum states. However, it is not yet clear how far one can go in this direction [8], and a complete understanding of how classical behavior emerges from the quantum substrate requires the design and the implementation of dedicated experiments. Examples of this kind are single-particle interference of macro-molecules [9], the demonstration of entanglement between collective spins of atomic ensembles [10], and of entanglement in Josephson-junction qubits [11]. For what concerns mechanical resonators, the experimental efforts are currently focusing on cooling them down to their motional ground state [2]. This goal has not been achieved yet, but promising results in this direction have been obtained in different setups [12,13,14,15,16,17,18,19,20,21,22,23,24,25,26,27,28,29,30,31], involving different examples of mechanical resonators coupled either to radiative or to electrical degrees of freedom. Ground state cooling of microgram-scale resonators seems to be within reach, as already suggested by various theoretical proposals [32,33,34,35,36,37,38,39,40,41,42,43] which showed how a mechanical oscillator can be coupled to another system so that the latter can act as an effective zero-temperature reservoir. In the first part of this chapter we shall review the problem of ground state cooling of a mechanical resonator, by focusing onto the case where the role of effective zero-temperature “fridge” is played by an optical cavity mode, coupled to the resonator by radiation pressure. In this case this interaction can be exploited for cooling in two different ways: i) back-action, or self-cooling [33,39,40,41,42,43] in which the off-resonant operation of the cavity results in a retarded back action on the mechanical system and hence in a “self”-modification of its dynamics [14,17,18,20,21,23,24,25,26,27,29,30,31]; ii) cold-damping quantum feedback, where the oscillator position is measured through a phase-sensitive detection of the cavity output and the resulting photocurrent is used for a real-time correction of the dynamics [12,16,19,22,28]. We shall compare the two approaches and see that while back-action cooling is optimized in the good cavity limit where the resonator frequency is larger than the cavity bandwidth, cold damping is preferable in the opposite regime of larger cavity bandwidths [41]. It should be noticed that the model Hamiltonian based on radiation pressure coupling between an optical cavity mode and one movable cavity mirror is quite general and immediately extendible to other situations, such as the toroidal microcavities of Refs. [20,25], the capacitively coupled systems of Refs. [23,27] and even atomic condensate systems [44].

From the theory side, the generation of other examples of quantum states of a micro-mechanical resonator has been also considered. The most relevant examples are given by squeezed and resonator-field (or atoms) entangled states. Squeezed states of nano-mechanical resonators [45] are potentially useful for

surpassing the standard quantum limit for position and force detection [5], and could be generated in different ways, either by coupling to a qubit [46], or by measurement and feedback schemes [36,47]. Entanglement is instead the characteristic element of quantum theory, because it is responsible for correlations between observables that cannot be understood on the basis of local realistic theories [48]. For this reason, there has been an increasing interest in establishing the conditions under which entanglement between macroscopic objects can arise. Relevant experimental demonstration in this directions are given by the entanglement between collective spins of atomic ensembles [10], and between Josephson-junction qubits [11]. Then, starting from the proposal of Ref. [49] in which two mirrors of a ring cavity are entangled by the radiation pressure of the cavity mode, many proposals involved nano- and micro-mechanical resonators, eventually entangled with other systems. One could entangle a nanomechanical oscillator with a Cooper-pair box [50], while Ref. [51] studied how to entangle an array of nanomechanical oscillators. Further proposals suggested to entangle two charge qubits [52] or two Josephson junctions [53] via nanomechanical resonators, or to entangle two nanomechanical resonators via trapped ions [54], Cooper pair boxes [55], or dc-SQUIDS [56]. More recently, schemes for entangling a superconducting coplanar waveguide field with a nanomechanical resonator, either via a Cooper pair box within the waveguide [57], or via direct capacitive coupling [58], have been proposed. After Ref. [49], other optomechanical systems have been proposed for entangling optical and/or mechanical modes by means of the radiation pressure interaction. Ref. [59] considered two mirrors of two different cavities illuminated with entangled light beams, while Refs. [60,61,62,63] considered different examples of double-cavity systems in which entanglement either between different mechanical modes, or between a cavity mode and a vibrational mode of a cavity mirror have been studied. Refs. [64,65] considered the simplest scheme capable of generating stationary optomechanical entanglement, i.e., a single Fabry-Perot cavity either with one [64], or both [65], movable mirrors.

In the second part of the chapter we shall focus on the generation of stationary entanglement by starting from the Fabry-Perot model of Ref. [64], which is remarkable for its simplicity and robustness against temperature, and extend its study in various directions. In fact, entangled optomechanical systems could be profitably used for the realization of quantum communication networks, in which the mechanical modes play the role of local nodes where quantum information can be stored and retrieved, and optical modes carry this information between the nodes. Refs. [66,67,68] proposed a scheme of this kind, based on free-space light modes scattered by a single reflecting mirror, which could allow the implementation of continuous variable (CV) quantum teleportation [66], quantum telecloning [67], and entanglement swapping [68]. Therefore, any quantum communication application involves *traveling output* modes rather than intracavity ones, and it is important to study how the optomechanical entanglement generated within the cavity is transferred to the output field.

Furthermore, by considering the output field, one can adopt a multiplexing approach because, by means of spectral filters, one can always select many different traveling output modes originating from a single intracavity mode. One can therefore manipulate a multipartite system, eventually possessing multipartite entanglement. We shall develop a general theory showing how the entanglement between the mechanical resonator and optical output modes can be properly defined and calculated [69]. We shall see that, together with its output field, the single Fabry-Perot cavity system of Ref. [64] represents the “cavity version” of the free-space scheme of Refs. [66,67]. In fact, as it happens in this latter scheme, all the relevant dynamics induced by radiation pressure interaction is carried by the two output modes corresponding to the first Stokes and anti-Stokes sidebands of the driving laser. In particular, the optomechanical entanglement with the intracavity mode is optimally transferred to the output Stokes sideband mode, which is however robustly entangled also with the anti-Stokes output mode. We shall see that the present Fabry-Perot cavity system is preferable with respect to the free space model of Refs. [66,67], because entanglement is achievable in a much more accessible experimental parameter region. We shall then extend the analysis to the case of a doubly-driven cavity mode. We shall see that a peculiar parameter regime exists where the optomechanical system, owing to the combined action of the two driven modes, is always stable and is characterized by robust entanglement between the resonator and the cavity output fields.

In the last Section we shall investigate the possibility to couple and entangle in a robust way optomechanical systems to atomic ensembles, in order to achieve a strongly-coupled hybrid multipartite system [70,71]. We shall see that this is indeed possible, especially when the atomic ensemble is resonant with the Stokes sideband induced by the resonator motion. Such hybrid systems might represent an important candidate for the realization of CV quantum interfaces within CV quantum information networks.

## 2 Cavity optomechanics via radiation pressure

The simplest cavity optomechanical system consists of a Fabry-Perot cavity with one heavy, fixed mirror through which a laser of frequency  $\omega_l$  drives a cavity mode, and another light end-mirror of mass  $m$  (typically in the micro or nanogram range), free to oscillate at some mechanical frequency  $\omega_m$ . Our treatment is however valid also for other cavity geometries in which one has an optical mode coupled by radiation pressure to a mechanical degree of freedom. A notable example is provided by silica toroidal optical microcavities which are coupled to radial vibrational modes of the supporting structure [20,72]. Radiation pressure typically excites several mechanical degrees of freedom of the system with different resonant frequencies. However, a single mechanical

mode can be considered when a bandpass filter in the detection scheme is used [73] and coupling between the different vibrational modes can be neglected. One has to consider more than one mechanical mode only when two close mechanical resonances fall within the detection bandwidth (see Ref. [74] for the effect of a nearby mechanical mode on cooling and entanglement). The Hamiltonian of the system describes two harmonic oscillators coupled via the radiation pressure interaction, and reads [75]

$$H = \hbar\omega_c a^\dagger a + \frac{1}{2}\hbar\omega_m(p^2 + q^2) - \hbar G_0 a^\dagger a q + i\hbar\mathcal{E}(a^\dagger e^{-i\omega_l t} - a e^{i\omega_l t}). \quad (1)$$

The first term describes the energy of the cavity mode, with lowering operator  $a$  ( $[a, a^\dagger] = 1$ ), frequency  $\omega_c$  (and therefore detuned by  $\Delta_0 = \omega_c - \omega_l$  from the laser), and decay rate  $\kappa$ . The second term gives the energy of the mechanical mode, described by dimensionless position and momentum operators  $q$  and  $p$  ( $[q, p] = i$ ). The third term is the radiation-pressure coupling of rate  $G_0 = (\omega_c/L)\sqrt{\hbar/m\omega_m}$ , where  $m$  is the effective mass of the mechanical mode [73], and  $L$  is an effective length that depends upon the cavity geometry: it coincides with the cavity length in the Fabry-Perot case, and with the toroid radius in the case of Refs. [20,72]. The last term describes the input driving by a laser with frequency  $\omega_l$ , where  $\mathcal{E}$  is related to the input laser power  $\mathcal{P}$  by  $|\mathcal{E}| = \sqrt{2\mathcal{P}\kappa/\hbar\omega_l}$ . One can adopt the single cavity mode description of Eq. (1) as long as one drives only one cavity mode and the mechanical frequency  $\omega_m$  is much smaller than the cavity free spectral range  $FSR \sim c/2L$ . In this case, in fact, scattering of photons from the driven mode into other cavity modes is negligible [76].

### 2.1 Langevin equations formalism

The dynamics are also determined by the fluctuation-dissipation processes affecting both the optical and the mechanical mode. They can be taken into account in a fully consistent way [75] by considering the following set of nonlinear QLE (quantum Langevin equations), written in a frame rotating at  $\omega_l$

$$\dot{q} = \omega_m p, \quad (2)$$

$$\dot{p} = -\omega_m q - \gamma_m p + G_0 a^\dagger a + \xi, \quad (3)$$

$$\dot{a} = -(\kappa + i\Delta_0)a + iG_0 a q + \mathcal{E} + \sqrt{2\kappa}a^{in}. \quad (4)$$

The mechanical mode is affected by a viscous force with damping rate  $\gamma_m$  and by a Brownian stochastic force with zero mean value  $\xi(t)$ , possessing the

correlation function [75,77]

$$\langle \xi(t)\xi(t') \rangle = \frac{\gamma_m}{\omega_m} \int \frac{d\omega}{2\pi} e^{-i\omega(t-t')} \omega \left[ \coth \left( \frac{\hbar\omega}{2k_B T_0} \right) + 1 \right], \quad (5)$$

where  $k_B$  is the Boltzmann constant and  $T_0$  is the temperature of the reservoir of the micromechanical oscillator. The correlation function and the commutator of the Gaussian stochastic force  $\xi(t)$  are not proportional to a Dirac delta and therefore  $\xi(t)$  is a non-Markovian stochastic process. This fact guarantees that the QLE of Eqs. (2)-(4) preserve the correct commutation relations between operators during the time evolution [75]. However, a Markovian description of the symmetrized correlations of  $\xi(t)$  is justified in two different limits, which are both met in typical experimental situations: i) not too low temperatures  $k_B T_0 / \hbar\omega_m \gg 1$ , which for typical values is satisfied even at cryogenic temperatures; ii) high mechanical quality factor  $Q = \omega_m / \gamma_m \rightarrow \infty$  [78], which is an important condition for the observation of quantum effects on the mechanical resonator. In this case the correlation function of Eq. (5) can be approximated as

$$\langle \xi(t)\xi(t') \rangle \simeq \gamma_m \left[ (2n_0 + 1)\delta(t - t') + i \frac{\delta'(t - t')}{\omega_m} \right], \quad (6)$$

where  $n_0 = (\exp\{\hbar\omega_m/k_B T_0\} - 1)^{-1}$  is the mean thermal excitation number of the resonator and  $\delta'(t - t')$  denotes the derivative of the Dirac delta.

The cavity mode amplitude instead decays at the rate  $\kappa$  and is affected by the vacuum radiation input noise  $a^{in}(t)$ , whose correlation functions are given by [79]

$$\langle a^{in}(t)a^{in,\dagger}(t') \rangle = [N(\omega_c) + 1] \delta(t - t'). \quad (7)$$

$$\langle a^{in,\dagger}(t)a^{in}(t') \rangle = N(\omega_c)\delta(t - t'), \quad (8)$$

where  $N(\omega_c) = (\exp\{\hbar\omega_c/k_B T_0\} - 1)^{-1}$  is the equilibrium mean thermal photon number. At optical frequencies  $\hbar\omega_c/k_B T_0 \gg 1$  and therefore  $N(\omega_c) \simeq 0$ , so that only the correlation function of Eq. (7) is relevant.

Equations (2)-(4) are not easy to analyze owing to the nonlinearity. However, one can proceed with a linearization of operators around the steady state. The semiclassical steady state is characterized by an intracavity field amplitude  $\alpha_s$  ( $|\alpha_s| \gg 1$ ), and a new equilibrium position for the oscillator, displaced by  $q_s$ . The parameters  $\alpha_s$  and  $q_s$  are the solutions of the nonlinear algebraic equations obtained by factorizing Eqs. (2)-(4) and setting the time derivatives to zero:

$$q_s = \frac{G_0 |\alpha_s|^2}{\omega_m}, \quad (9)$$

$$\alpha_s = \frac{\mathcal{E}}{\kappa + i\Delta}, \quad (10)$$

where the latter equation is in fact the nonlinear equation determining  $\alpha_s$ , since the effective cavity detuning  $\Delta$ , including radiation pressure effects, is given by [80]

$$\Delta = \Delta_0 - \frac{G_0^2 |\alpha_s|^2}{\omega_m}. \quad (11)$$

Rewriting each Heisenberg operator of Eqs. (2)-(4) as the c-number steady state value plus an additional fluctuation operator with zero mean value, one gets the exact QLE for the fluctuations

$$\delta\dot{q} = \omega_m \delta p, \quad (12)$$

$$\delta\dot{p} = -\omega_m \delta q - \gamma_m \delta p + G_0 (\alpha_s \delta a^\dagger + \alpha_s^* \delta a) + \delta a^\dagger \delta a + \xi, \quad (13)$$

$$\delta\dot{a} = -(\kappa + i\Delta) \delta a + iG_0 (\alpha_s + \delta a) \delta q + \sqrt{2\kappa} a^{in}. \quad (14)$$

Since we have assumed  $|\alpha_s| \gg 1$ , one can safely neglect the nonlinear terms  $\delta a^\dagger \delta a$  and  $\delta a \delta q$  in the equations above, and get the linearized QLE

$$\delta\dot{q} = \omega_m \delta p, \quad (15)$$

$$\delta\dot{p} = -\omega_m \delta q - \gamma_m \delta p + G \delta X + \xi, \quad (16)$$

$$\delta\dot{X} = -\kappa \delta X + \Delta \delta Y + \sqrt{2\kappa} X^{in}, \quad (17)$$

$$\delta\dot{Y} = -\kappa \delta Y - \Delta \delta X + G \delta q + \sqrt{2\kappa} Y^{in}. \quad (18)$$

Here we have chosen the phase reference of the cavity field so that  $\alpha_s$  is real and positive, we have defined the cavity field quadratures  $\delta X \equiv (\delta a + \delta a^\dagger)/\sqrt{2}$  and  $\delta Y \equiv (\delta a - \delta a^\dagger)/i\sqrt{2}$  and the corresponding Hermitian input noise operators  $X^{in} \equiv (a^{in} + a^{in,\dagger})/\sqrt{2}$  and  $Y^{in} \equiv (a^{in} - a^{in,\dagger})/i\sqrt{2}$ . The linearized QLE show that the mechanical mode is coupled to the cavity mode quadrature fluctuations by the effective optomechanical coupling

$$G = G_0 \alpha_s \sqrt{2} = \frac{2\omega_c}{L} \sqrt{\frac{\mathcal{P}\kappa}{m\omega_m\omega_l(\kappa^2 + \Delta^2)}}, \quad (19)$$

which can be made very large by increasing the intracavity amplitude  $\alpha_s$ . Notice that together with the condition  $\omega_m \ll c/L$  which is required for the single cavity mode description,  $|\alpha_s| \gg 1$  is the *only* assumption required by the linearized approach. This is in contrast with the perturbative approaches described in [40], where a reduced master equation of the mechanical resonator is derived under the weak-coupling assumption  $G \ll \omega_m$ .



## 2.2 Stability analysis

The stability analysis can be performed on the linearized set of equations Eqs. (2)-(4) by using the Routh-Hurwitz criterion [81]. Two conditions are obtained

$$s_1 = 2\gamma_m\kappa \left\{ \left[ \kappa^2 + (\omega_m - \Delta)^2 \right] \left[ \kappa^2 + (\omega_m + \Delta)^2 \right] \right. \quad (20)$$

$$\left. + \gamma_m \left[ (\gamma_m + 2\kappa) (\kappa^2 + \Delta^2) + 2\kappa\omega_m^2 \right] \right\} + \Delta\omega_m G^2 (\gamma_m + 2\kappa)^2 > 0, \quad (21)$$

$$s_2 = \omega_m (\kappa^2 + \Delta^2) - G^2\Delta > 0. \quad (22)$$

The violation of the first condition,  $s_1 < 0$ , indicates instability in the domain of blue-detuned laser ( $\Delta < 0$ ) and it corresponds to the emergence of a self-sustained oscillation regime where the mirror effective damping rate vanishes. In this regime, the laser field energy leaks into field harmonics at frequencies  $\omega_l \pm r\omega_m$  ( $r = 1, 2, \dots$ ) and also feeds the mirror coherent oscillations. A complex multistable regime can emerge as described in [82]. The violation of the second condition  $s_2 < 0$  indicates the emergence of the well-known effect of bistable behavior observed in [83] and occurs only for positive detunings ( $\Delta > 0$ ). In the following we restrict our analysis to positive detunings in the stable regime where both  $s_1$  and  $s_2$  conditions are fulfilled. A parametric plot showing the domain of stability in the red-detuning regime  $\Delta > 0$  is shown in Fig. 1 where we have plotted the stability parameter

$$\eta = 1 - \frac{G^2\Delta}{\omega_m (\kappa^2 + \Delta^2)}. \quad (23)$$

Negative values of  $\eta$  indicate the emergence of instability. We have chosen the following set of parameters which will be used extensively throughout the chapter and which is denoted by  $p_0 = (\omega_m, Q_m, m, L, \lambda_c, T_0) = (2\pi \times 10 \text{ MHz}, 10^5, 30 \text{ ng}, 0.5 \text{ mm}, 1064 \text{ nm}, 0.6 \text{ K})$ . These values are comparable to those used in recent experiments [17,18,19,24,25,26,30,31].

## 2.3 Covariance matrix and logarithmic negativity

The mechanical and intracavity optical mode form a bipartite continuous variable (CV) system. We are interested in the properties of its steady state which, due to the linearized treatment and to the Gaussian nature of the noise operators, is a zero-mean Gaussian state, completely characterized by its symmetrized covariance matrix (CM). The latter is given by the  $4 \times 4$  matrix with elements

$$\mathcal{V}_{lm} = \frac{\langle u_l(\infty) u_m(\infty) + u_m(\infty) u_l(\infty) \rangle}{2}, \quad (24)$$

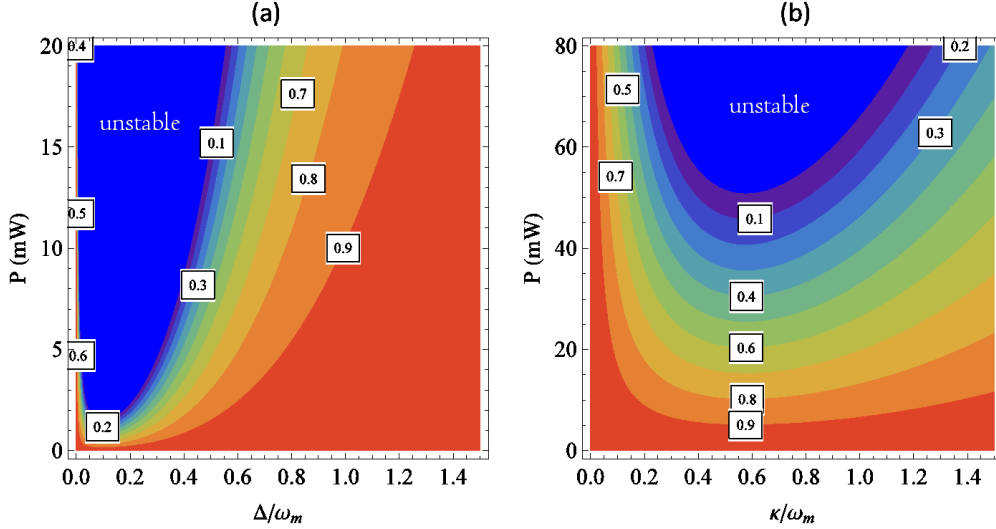


Fig. 1. Stability condition in the red-detuning region. (a) Contour plot of the stability parameter  $\eta$  of Eq. (23) as a function of input power  $\mathcal{P}$  and normalized detuning  $\Delta/\omega_m$ . The parameter set  $p_0=(\omega_m, Q_m, m, L, \lambda_c, T_0) = (2\pi \times 10 \text{ MHz}, 10^5, 30 \text{ ng}, 0.5 \text{ mm}, 1064 \text{ nm}, 0.6 \text{ K})$  has been used, together with  $\mathcal{F} = 8 \times 10^4$  (corresponding to  $\kappa = 0.37\omega_m$ ). The blue area corresponds to the unstable regime. (b) Stability parameter  $\eta$  versus  $\mathcal{P}$  and the normalized cavity decay rate  $\kappa/\omega_m$  at  $\Delta = \omega_m$ .

where  $u_m(\infty)$  is the asymptotic value of the  $m$ -th component of the vector of quadrature fluctuations

$$u(t) = (\delta q(t), \delta p(t), \delta X(t), \delta Y(t))^T. \quad (25)$$

Its time evolution is given by Eqs. (15)-(18), which can be rewritten in compact form as

$$\frac{d}{dt}u(t) = Au(t) + v(t), \quad (26)$$

with  $A$  the drift matrix

$$A = \begin{pmatrix} 0 & \omega_m & 0 & 0 \\ -\omega_m & -\gamma_m & G & 0 \\ 0 & 0 & -\kappa & \Delta \\ G & 0 & -\Delta & -\kappa \end{pmatrix}, \quad (27)$$

and  $v(t)$  the vector of noises

$$v(t) = (0, \xi(t), \sqrt{2\kappa}X^{in}(t), \sqrt{2\kappa}Y^{in}(t))^T. \quad (28)$$

The steady state CM can be determined by solving the Lyapunov equation

$$A\mathcal{V} + \mathcal{V}A^T = -D, \quad (29)$$

where  $D$  is the  $4 \times 4$  diffusion matrix which characterizes the noise correlations and is defined by the relation  $\langle n_l(t) n_m(t') + n_m(t') n_l(t) \rangle / 2 = D_{lm} \delta(t - t')$ . Using Eqs. (6)-(7),  $D$  can be written as

$$D = \text{diag}[0, \gamma_m(2n_0 + 1), \kappa, \kappa]. \quad (30)$$

Eq. (29) is a linear equation for  $\mathcal{V}$  and it can be straightforwardly solved, but the general exact expression is very cumbersome and will not be reported here.

The CM allows to calculate also the entanglement of the steady state. We adopt as entanglement measure the logarithmic negativity  $E_{\mathcal{N}}$ , which is defined as [84]

$$E_{\mathcal{N}} = \max[0, -\ln 2\eta^-]. \quad (31)$$

Here  $\eta^- \equiv 2^{-1/2} [\Sigma(\mathcal{V}) - [\Sigma(\mathcal{V})^2 - 4 \det \mathcal{V}]^{1/2}]^{1/2}$  and  $\Sigma(\mathcal{V}) \equiv \det \mathcal{V}_1 + \det \mathcal{V}_2 - 2 \det \mathcal{V}_c$ , with  $\mathcal{V}_1, \mathcal{V}_2$  and  $\mathcal{V}_c$  being  $2 \times 2$  block matrices of

$$\mathcal{V} \equiv \begin{pmatrix} \mathcal{V}_1 & \mathcal{V}_c \\ \mathcal{V}_c^T & \mathcal{V}_2 \end{pmatrix}. \quad (32)$$

A bimodal Gaussian state is entangled if and only if  $\eta^- < 1/2$ , which is equivalent to Simon's necessary and sufficient entanglement non-positive partial transpose criterion for Gaussian states [85], which can be written as  $4 \det \mathcal{V} < \Sigma(\mathcal{V}) - 1/4$ . Logarithmic negativity is a convenient entanglement measure because it is the only one which can always be explicitly computed and it is also additive. The drawback of  $E_{\mathcal{N}}$  is that, differently from the entanglement of formation and the distillable entanglement, it is not strongly super-additive and therefore it cannot be used to provide lower-bound estimates of the entanglement of a generic state by evaluating the entanglement of Gaussian state with the same correlation matrix [86]. This fact however is not important in our case because the steady state of the system is Gaussian within the validity limit of our linearization procedure.

### 3 Ground state cooling

The steady state CM  $\mathcal{V}$  determines also the mean energy of the mechanical resonator, which is given by

$$U = \frac{\hbar\omega_m}{2} [\langle \delta q^2 \rangle + \langle \delta p^2 \rangle] = \frac{\hbar\omega_m}{2} [\mathcal{V}_{11} + \mathcal{V}_{22}] \equiv \hbar\omega_m \left( n + \frac{1}{2} \right), \quad (33)$$

where  $n = (\exp\{\hbar\omega_m/k_B T\} - 1)^{-1}$  is the occupancy corresponding to a bath temperature  $T$ . Obviously, in the absence of coupling to the cavity field it is  $n = n_0$ , where  $n_0$  corresponds to the actual temperature of the environment  $T_0$ .

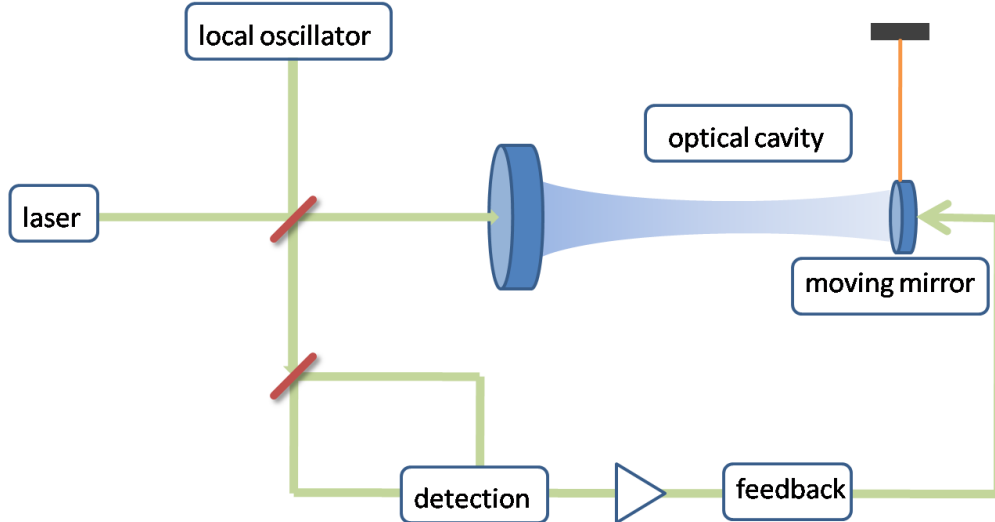


Fig. 2. Setup for feedback cooling (cold damping). The cavity output field is homodyne detected (thus acquiring information about the mirror position) and a force proportional to its derivative is fed back to the mirror.

The optomechanical coupling with the cavity mode can be used to ‘engineer’ an effective bath of much lower temperature  $T \ll T_0$ , so that the mechanical resonator is cooled. Let us see when it is possible to reach the ideal condition  $n \ll 1$ , which corresponds to ground state cooling.

### 3.1 Feedback cooling

A simple way for cooling an object is to continuously detect its momentum and apply ‘corrective kicks’ that continuously reduce it eventually to zero [32,35,36]. This is the idea of feedback cooling illustrated in Fig. 2 where the mirror position is detected via phase-sensitive homodyne detection of the cavity output field and a force proportional to the time derivative of the output signal (thus to the velocity) is fed back to it. By Fourier transforming Eq. (18) one obtains

$$\delta Y(\omega) = \frac{G(\kappa - i\omega)}{(\kappa - i\omega)^2 + \Delta^2} \delta q(\omega) + \text{noise terms}, \quad (34)$$

which shows that the intracavity phase-quadrature is sensitive to the mirror motion and moreover its optimal sensitivity is reached at resonance, when  $\Delta = 0$ . In this latter condition  $\delta X(\omega)$  is not sensitive to the mirror motion, suggesting that the strongest feedback effect is obtained by detecting the output phase-quadrature  $Y^{out}$  and feeding it back to the resonator.

### 3.1.1 Phase quadrature feedback

As a consequence we set  $\Delta = 0$  and add a feedback force in Eq. (16) so that

$$\delta\dot{p} = -\omega_m\delta q - \gamma_m\delta p + G\delta X + \xi - \int_{-\infty}^t ds g(t-s)\delta Y^{est}(s), \quad (35)$$

where  $Y^{est}(s)$  is the estimated intracavity phase-quadrature, which, using input-output relations [79] and focusing onto the ideal scenario of perfect detection, is given by

$$\delta Y^{est}(t) = \frac{Y^{out}(t)}{\sqrt{2\kappa}} = \delta Y(t) - \frac{Y^{in}(t)}{\sqrt{2\kappa}}. \quad (36)$$

The filter function  $g(t)$  is a causal kernel and  $g(\omega)$  is its Fourier transform. We choose a simple standard derivative high-pass filter

$$g(t) = g_{cd} \frac{d}{dt} [\theta(t)\omega_{fb}e^{-\omega_{fb}t}] \quad g(\omega) = \frac{-i\omega g_{cd}}{1 - i\omega/\omega_{fb}}, \quad (37)$$

so that  $\omega_{fb}^{-1}$  plays the role of the time delay of the feedback loop, and  $g_{cd} > 0$  is the feedback gain. The ideal derivative limit is obtained when  $\omega_{fb} \rightarrow \infty$ , implying  $g(\omega) = -i\omega g_{cd}$  and therefore  $g(t) = g_{cd}\delta'(t)$ . In this limit the feedback force is equal (apart from an additional noise term) to  $-g_{cd}\delta\dot{Y}$  which, due to Eq. (34), is an additional viscous force  $-(g_{cd}G/\kappa)\delta\dot{q}$  only in the bad cavity limit  $\kappa \gg \omega_m, \gamma_m$ .

One can solve the Langevin equations supplemented with the feedback term in the Fourier domain. In fact, the two steady state oscillator variances  $\langle \delta q^2 \rangle$  and  $\langle \delta p^2 \rangle$  can be expressed by the following frequency integrals

$$\langle \delta q^2 \rangle = \int_{-\infty}^{\infty} \frac{d\omega}{2\pi} S_q^{cd}(\omega), \quad \langle \delta p^2 \rangle = \int_{-\infty}^{\infty} \frac{d\omega}{2\pi} \frac{\omega^2}{\omega_m^2} S_q^{cd}(\omega), \quad (38)$$

where  $S_q^{cd}(\omega)$  is the position noise spectrum. Its explicit expression is given by

$$S_q^{cd}(\omega) = |\chi_{eff}^{cd}(\omega)|^2 [S_{th}(\omega) + S_{rp}(\omega) + S_{fb}(\omega)], \quad (39)$$

where the thermal, radiation pressure and feedback-induced contributions are respectively given by

$$S_{th}(\omega) = \frac{\gamma_m\omega}{\omega_m} \coth\left(\frac{\hbar\omega}{2k_B T_0}\right), \quad (40)$$

$$S_{rp}(\omega) = \frac{G^2\kappa}{\kappa^2 + \omega^2}, \quad (41)$$

$$S_{fb}(\omega) = \frac{|g(\omega)|^2}{4\kappa} \quad (42)$$

and  $\chi_{eff}^{cd}(\omega)$  is the susceptibility of the mechanical oscillator modified by the feedback

$$\chi_{eff}^{cd}(\omega) = \omega_m \left[ \omega_m^2 - \omega^2 - i\omega\gamma_m + \frac{g(\omega)G\omega_m}{\kappa - i\omega} \right]^{-1}. \quad (43)$$

This effective susceptibility contains the relevant physics of cold damping. In fact it can be rewritten as the susceptibility of an harmonic oscillator with effective (frequency-dependent) damping and oscillation frequency. The modification of resonance frequency (optical spring effect [21,36]) is typically small for the chosen parameter regime ( $\omega_m \simeq 1$  MHz) and the only relevant effect of feedback is the modification of the mechanical damping which, in the case of the choice of Eq. (37), is given by

$$\gamma_m^{eff,cd}(\omega) = \gamma_m + \frac{g_{cd}G\omega_m\omega_{fb}(\kappa\omega_{fb} - \omega^2)}{(\kappa^2 + \omega^2)(\omega_{fb}^2 + \omega^2)}. \quad (44)$$

This expression shows that the damping of the oscillator may be significantly increased due to the combined action of feedback and of radiation pressure coupling to the field. In the ideal limit of instantaneous feedback and of a bad cavity,  $\kappa, \omega_{fb} \gg \omega_m, \gamma_m$ , effective damping is frequency-independent and given by  $\gamma_m^{eff,cd} \simeq \gamma_m + g_{cd}G\omega_m/\kappa = \gamma_m(1 + g_2)$ , where we have defined the scaled, dimensionless feedback gain  $g_2 \equiv g_{cd}G\omega_m/\kappa\gamma_m$  [36].

The presence of cold-damping feedback also modifies the stability conditions. The Routh-Hurwitz criteria are equivalent to the conditions that all the poles of the effective susceptibility of Eq. (43) are in the lower complex half-plane. For the choice of Eq. (37) there is only one non-trivial stability condition, which reads

$$s_{cd} = \left[ \gamma_m\kappa\omega_{fb} + g_{cd}G\omega_m\omega_{fb} + \omega_m^2(\kappa + \omega_{fb}) \right] \left[ (\kappa + \gamma_m)(\kappa + \omega_{fb})(\gamma_m + \omega_{fb}) + \gamma_m\omega_m^2 - g_{cd}G\omega_m\omega_{fb} \right] - \kappa\omega_m^2\omega_{fb}(\kappa + \gamma_m + \omega_{fb})^2 > 0. \quad (45)$$

This condition shows that the system may become unstable for large gain and finite feedback delay-time and cavity bandwidth because in this limit the feedback force can be out-of-phase with the oscillator motion and become an accelerating rather than a viscous force [41].

The performance of cold-damping feedback for reaching ground state cooling is analyzed in detail in Ref. [41], which shows that the optimal parameter regime is  $\kappa \gg \omega_{fb} \sim \omega_m \gg \gamma_m$ , which correspond to a bad-cavity limit and a finite-bandwidth feedback, i.e., with a feedback delay-time comparable to the resonator frequency. One gets in this case

$$\langle \delta q^2 \rangle \simeq \left[ 1 + g_2 + \frac{\omega_{fb}^2}{\omega_m^2} \right]^{-1} \left[ \frac{g_2^2}{4\zeta} + \left( n_0 + \frac{1}{2} + \frac{\zeta}{4} \right) \left( 1 + \frac{\omega_m^2}{\omega_{fb}^2} \right) \right] \quad (46)$$

$$\begin{aligned} \langle \delta p^2 \rangle \simeq & \left[ 1 + g_2 + \frac{\omega_m^2}{\omega_{fb}^2} \right]^{-1} \left[ \frac{g_2^2}{4\zeta} \left( 1 + \frac{g_2 \gamma_m \omega_{fb}}{\omega_m^2} \right) \right. \\ & \left. + \left( n_0 + \frac{1}{2} + \frac{\zeta}{4} \right) \left( 1 + \frac{\omega_m^2}{\omega_{fb}^2} + \frac{g_2 \gamma_m}{\omega_{fb}} \right) \right], \end{aligned} \quad (47)$$

where we have defined the scaled dimensionless input power  $\zeta = 2G^2/\kappa\gamma_m$ . These two expressions show that with cold-damping feedback,  $\langle \delta q^2 \rangle \neq \langle \delta p^2 \rangle$ , i.e., energy equipartition does not hold anymore. The best cooling regime is achieved for  $\omega_{fb} \sim 3\omega_m$  and  $g_2 \simeq \xi$  (i.e.  $g_{cd} \simeq 2G/\omega_m$ ), i.e. for *large but finite* feedback gain [35,36,41]. This is consistent with the fact that stability imposes an upper bound to the feedback gain when  $\kappa$  and  $\omega_{fb}$  are finite. The optimal cooling regime for cold damping is illustrated in Fig. 3a, where  $n$  is plotted versus the feedback gain  $g_{cd}$  and the input power  $P$ , at fixed  $\kappa = 5\omega_m$  (bad-cavity condition) and  $\omega_{fb} = 3.5\omega_m$ . Fig. 3b instead explicitly shows the violation of the equipartition condition even in this regime close to ground state (the feedback gain is fixed at the value  $g_{cd} = 1.2$ ): the resonator is in a position-squeezed thermal state corresponding to a very low effective temperature.

### 3.1.2 Generalized quadrature feedback

The above analysis shows that cold-damping feedback better cools the mechanical resonator when the feedback is not instantaneous and therefore the feedback force is not a simple viscous force. This suggests that one can further optimize feedback cooling by considering a *generalized* estimated quadrature which is a combination of phase and amplitude field quadratures. In fact one may expect that in the optimal regime, the information provided by the amplitude quadrature  $X^{out}(t)$  is also useful.

Therefore, in order to optimize cooling via feedback, we apply a feedback force involving a generalized estimated quadrature

$$\delta Y_\theta^{est}(t) = \frac{Y^{out}(t) \cos \theta + X^{out}(t) \sin \theta}{\sqrt{2\kappa}}, \quad (48)$$

which is a linear combination of  $Y^{out}(t)$  and  $X^{out}(t)$  and where  $\theta$  is a detection phase which has to be optimized. The adoption of the new estimated quadrature leads to three effects: i) a modification of the expression for  $\chi_{eff}^{cd}(\omega)$  of Eq. (43) where  $g(\omega)$  is replaced by  $g(\omega) \cos \theta$ ; ii) a consequent reduction of the feedback-induced shot noise term  $S_{fb}(\omega)$ ; iii) a reduction of radiation pressure noise. In fact, the radiation pressure and feedback-induced noise contributions become

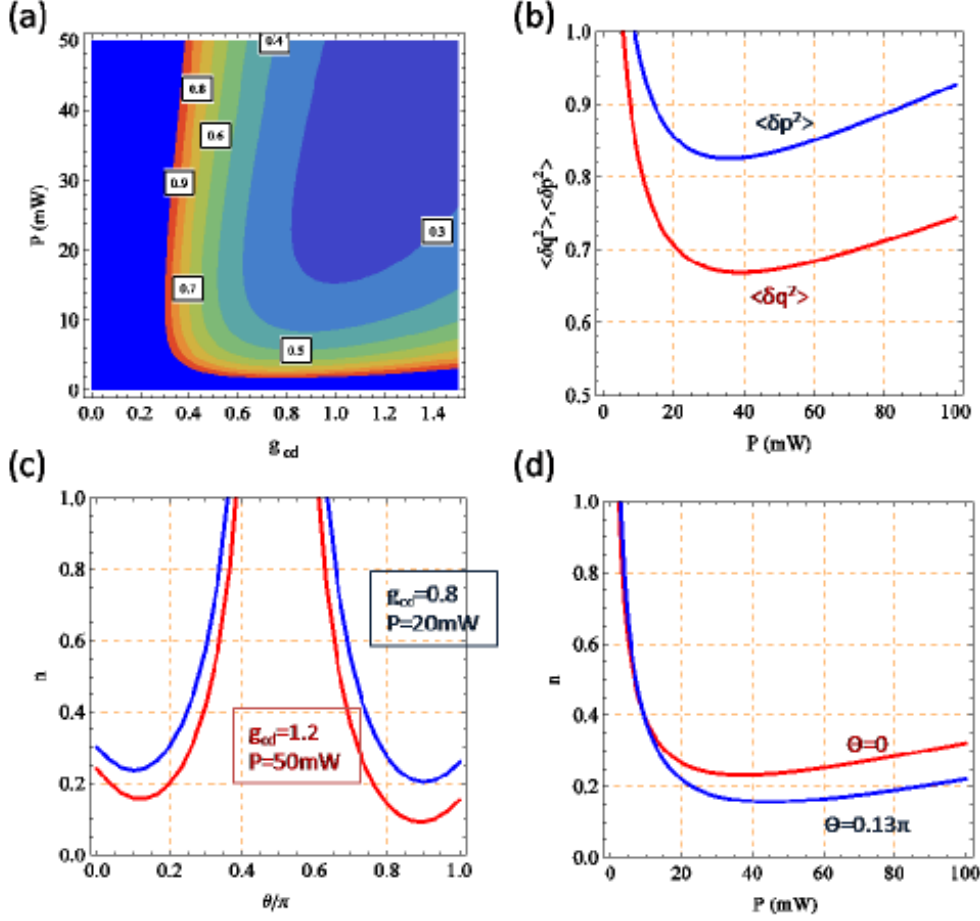


Fig. 3. Feedback cooling. (a) Contour plot of  $n$  as a function of  $\mathcal{P}$  and  $g_{cd}$ . The parameters are  $p_0$ ,  $\kappa = 5\omega_m$  and  $\omega_{fb} = 3.5\omega_m$ . (b) Illustration of the violation of energy equipartition around the optimal cooling regime. Parameters as before with  $g_{cd} = 1.2$ . (c)  $n$  versus the phase of the generalized quadrature  $\theta$  for two sets of  $g_{cd}$  and  $\mathcal{P}$ : the (upper) blue curve corresponds to  $g_{cd} = 0.8$  and  $\mathcal{P} = 20$  mW, while the (lower) red curve corresponds to  $g_{cd} = 1.2$  and  $\mathcal{P} = 50$  mW. (d) Comparison of  $n$  versus the input power  $\mathcal{P}$  between the case of standard cold damping feedback  $\theta = 0$  (upper red curve) and at a generalized detected quadrature with phase  $\theta = 0.13\pi$  (lower blue curve). Parameters as before, with  $g_{cd} = 1.2$ .

$$S_{rp}^\theta(\omega) = \frac{G^2\kappa}{\kappa^2 + \omega^2} \left| 1 - \frac{g(\omega) \sin \theta}{2G\kappa} (\kappa + i\omega) \right|^2, \quad (49)$$

$$S_{fb}^\theta(\omega) = \frac{|g(\omega)|^2}{4\kappa} \cos^2 \theta. \quad (50)$$

An improvement over the standard cold-damping feedback scheme can be obtained when the shot noise reduction effect predominates over the reduction of the effective damping due to feedback. This can be seen in Fig. (3c) where for two different choices for  $g_{cd}$  and  $\mathcal{P}$ , the occupancy  $n$  is plotted versus  $\theta$ . For one of these optimal phases,  $\theta_{opt} = 0.13\pi$ , we plot in Fig. (3d)  $n$  as a function of  $\mathcal{P}$  and compare it with the results of the standard phase quadrature feedback



to conclude that improvement via detection of a rotated output quadrature is indeed possible.

### 3.2 Back-action cooling

In analogy with well-known methods of atom and ion cooling [87,88], one can also think of cooling the mechanical resonator by exploiting its coherent coupling to a fast decaying system which provides an additional dissipation channel and thus cooling. In the present situation, radiation pressure couples the resonator with the cavity mode and the fast decaying channel is provided by the cavity photon loss rate  $\kappa$ . An equivalent description of the process can be given in terms of dynamical backaction [5,33]: the cavity reacts with a delay to the mirror motion and induces correlations between the radiation pressure force and the Brownian motion that lead to cooling or amplification, depending on the laser detuning. A quantitative description is provided by considering scattering of laser photons into the motional sidebands induced by the mirror motion (see Fig. 4) [39,40,41]. Stokes (red) and anti-Stokes (blue) sidebands are generated in the cavity at frequencies  $\omega_l \pm \omega_m$ . Laser photons are scattered by the moving oscillator into the two sidebands with rates

$$A_{\pm} = \frac{G^2 \kappa}{2 [\kappa^2 + (\Delta \pm \omega_m)^2]}, \quad (51)$$

simultaneously with the absorption (Stokes,  $A_+$ ) or emission (anti-Stokes,  $A_-$ ) of vibrational phonons. The inequality  $A_- > A_+$  leads to a decrease in the oscillator phonon occupation number and thus to cooling. Eq. (51) shows that this occurs when  $\Delta > 0$  and that an effective optical cooling rate,

$$\Gamma = A_- - A_+ = \frac{2G^2 \Delta \omega_m \kappa}{[\kappa^2 + (\omega_m - \Delta)^2] [\kappa^2 + (\omega_m + \Delta)^2]}, \quad (52)$$

can be defined, providing a measure of the coupling rate of the resonator with the effective zero-temperature environment represented by the decaying cavity mode. Since the mechanical damping rate  $\gamma_m$  is the coupling rate with the thermal reservoir of the resonator, one can already estimate that, when  $\Gamma \gg \gamma_m$ , the mechanical oscillator is cooled at the new temperature  $T \simeq (\gamma_m/\Gamma) T_0$ .

One can perform a more precise and rigorous derivation of the cooling rate and steady state occupancy by using Eq. (33). The position and momentum variances can be in fact obtained by solving Eq. (29) or, equivalently, by solving the linearized QLE in the Fourier domain and integrating the resulting noise spectra. The result of these calculations, in the limit of large mechanical quality factor  $Q_m$ , reads

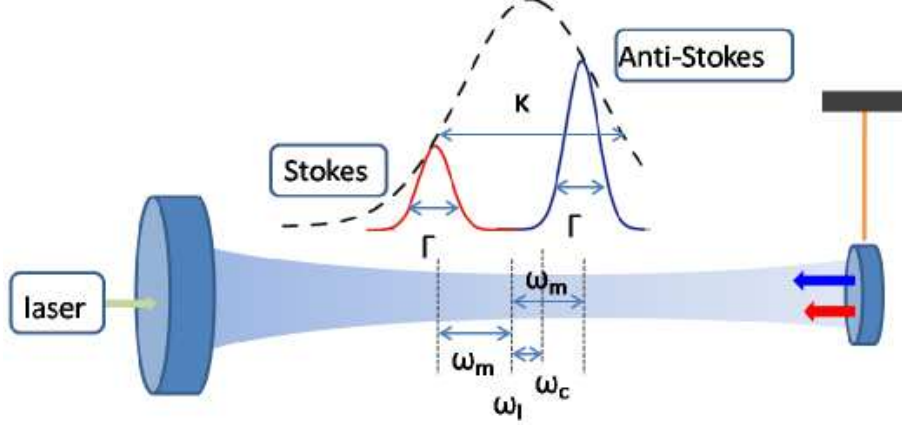


Fig. 4. Setup for cavity backaction cooling. Optical sidebands are scattered unevenly by the moving mirror. When the anti-Stokes sideband is resonant with the cavity ( $\Delta = \omega_m$ ), an effective flow of energy from the mirror out of the cavity leads to an effective cooling.

$$\langle \delta p^2 \rangle = \frac{1}{\gamma_m + \Gamma} \left\{ \frac{A_+ + A_-}{2} + \gamma_m n_0 \left( 1 + \frac{\Gamma}{2\kappa} \right) \right\}, \quad (53)$$

$$\langle \delta q^2 \rangle = \frac{1}{\gamma_m + \Gamma} \left\{ a \frac{A_+ + A_-}{2} + \frac{\gamma_m n_0}{\eta} \left( 1 + \frac{\Gamma}{2\kappa} b \right) \right\}, \quad (54)$$

where  $\eta$  is given by Eq. (23),

$$a = \frac{\kappa^2 + \Delta^2 + \eta \omega_m^2}{\eta (\kappa^2 + \Delta^2 + \omega_m^2)}, \quad (55)$$

$$b = \frac{2(\Delta^2 - \kappa^2) - \omega_m^2}{\kappa^2 + \Delta^2}. \quad (56)$$

In the perturbative limit  $\omega_m \gg n_0 \gamma_m, G$  and  $\kappa \gg \gamma_m, G$ , Eqs. (53)-(54) simplify to  $\langle \delta q^2 \rangle \simeq \langle \delta p^2 \rangle \simeq n + 1/2$ , with  $n \simeq [\gamma_m n_0 + A_+] / [\gamma_m + \Gamma]$ , which reproduces the result of [39,40]. This indicates that ground state cooling is reachable when  $\gamma_m n_0 < \Gamma$  and provided that the radiation pressure noise contribution  $A_+/\Gamma \simeq \kappa^2/(4\omega_m^2)$  is also small. The optical damping rate  $\Gamma$  can be increased by cranking up the input cavity power and thus  $G$ . However, when one considers the limitations imposed by the stability condition  $\eta > 0$ , one finds that there is an upper bound for  $G$  and consequently  $\Gamma$ . This is shown in Figs. 5a-5c, where one sees that for the chosen parameter regime  $p_0$ , optimal cooling is achieved for  $\Delta \simeq \omega_m$  (when the anti-Stokes sideband is resonant with the cavity, as expected), and in a moderate good-cavity condition,  $\kappa/\omega_m \simeq 0.2$ . Fig. 5b shows that close to this optimal cooling condition, equipartition is soon violated when the input power (and therefore the effective coupling  $G$ ) is further increased: the position variance becomes much larger than the momentum variance and it is divergent at the bistability threshold (see Eq. (54)).

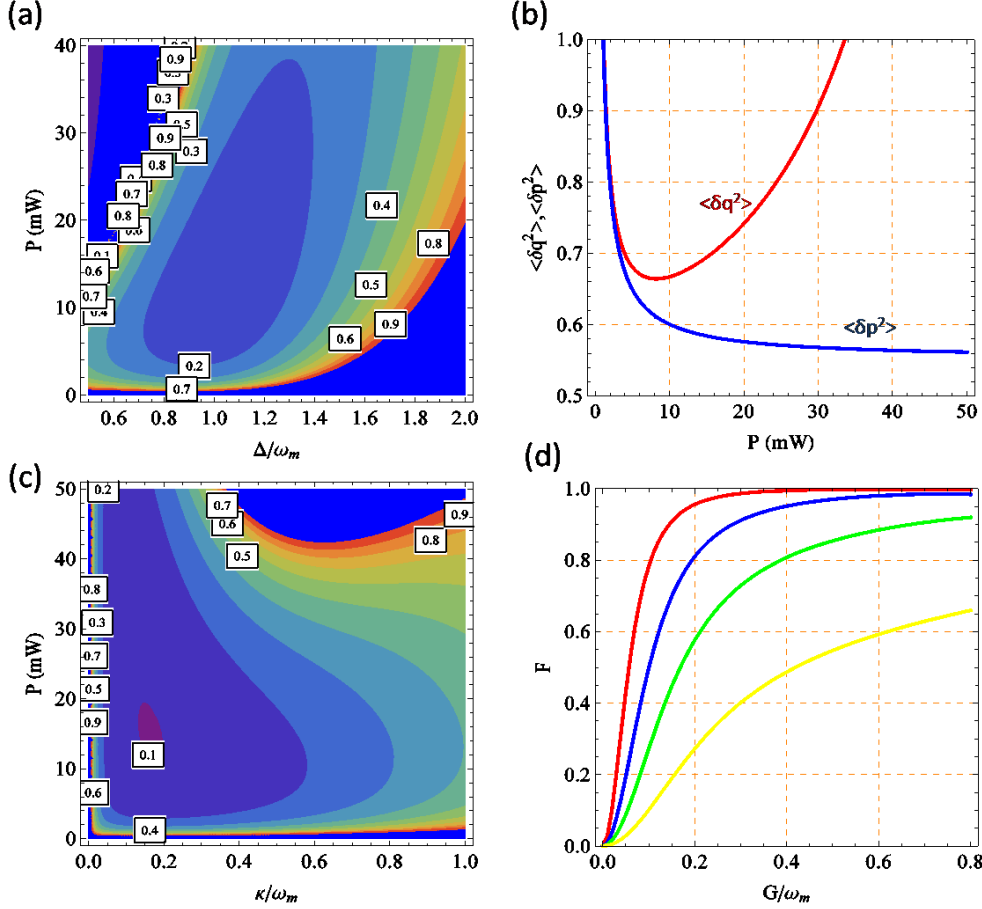


Fig. 5. Back action cooling. (a) Contour plot of  $n$  versus  $\Delta/\omega_m$  and  $\mathcal{P}$ . The parameters are  $p_0$  and  $\kappa = 0.37\omega_m$ . Optimal cooling is seen to emerge around  $\Delta = \omega_m$ . (b) For large  $\mathcal{P}$  extra shot-noise is fed-back into the position variance and the mirror thermalizes in a state where the equipartition theorem does not hold. (c) Contour plot of  $n$  vs.  $\kappa/\omega_m$  and  $\mathcal{P}$  for  $\Delta = \omega_m$ . Optimal cooling is achieved around  $\kappa \simeq 0.2 \times \omega_m$ . (d) Fidelity between the mirror and intracavity states in the cooling regime as a function of increasing intensity  $G/\omega_m$  with different values of  $\kappa/\omega_m = 0.2$  (red line), 0.5 (blue), 1 (green) and 2 (yellow).

### 3.3 Readout of the mechanical resonator state

Eq. (34) shows that the cavity output is sensitive to the resonator position. Therefore, after an appropriate calibration, the cavity output noise power spectrum provides a direct measurement of the position noise spectrum  $S_q(\omega)$  which, when integrated over  $\omega$ , yields the value of the position variance (see Eq. (38)). In many experiments [16,17,18,19,20,21,22,23,24,26], this value is employed to estimate the final effective temperature of the cooled resonator by assuming energy equipartition  $\langle \delta p^2 \rangle \simeq \langle \delta q^2 \rangle$  so that  $n \simeq \langle \delta q^2 \rangle - 1/2$ . However, as we have seen above (see Eqs. (46), (47), (53), (54)), equipartition does not generally hold and one should rather estimate  $\langle \delta p^2 \rangle$  from  $S_q(\omega)$  using

Eq. (38), or directly measure independently the resonator momentum. A different and more direct way of measuring the resonator temperature, borrowed from trapped-ion experiments [88], has been demonstrated in [25]: if the two motional sidebands are well resolved and detected via heterodyne measurement, the height of the two sideband peaks is proportional to  $n$  and to  $n + 1$ , so that one can directly measure the occupancy  $n$  from the comparison of the two peaks.

However, one should devise a scheme capable of reconstructing the *complete quantum state* of the resonator from the cavity output light, which is the only accessible degree of freedom carrying out information about it. In fact, the full reconstruction of the quantum state of the resonator is a necessary condition for the unambiguous demonstration of the quantum behavior of the mechanical resonator, as for example stationary entanglement, which will be discussed in the following. A scheme of this kind has been proposed in [64], based on the transfer of the resonator state onto the output field of an additional, fast-decaying, “probe” cavity mode. In fact, the annihilation operator of this probe cavity mode,  $a_p$ , obeys an equation analogous to the linearization of Eq. (14),

$$\delta\dot{a}_p = -(\kappa_p + i\Delta_p)\delta a_p + iG_p\alpha_p\delta q + \sqrt{2\kappa_2}a_p^{in}(t), \quad (57)$$

where  $\kappa_p$ ,  $\Delta_p$ ,  $G_p$ ,  $\alpha_p$ , and  $a_p^{in}(t)$  are respectively the decay rate, the effective detuning, the coupling, the intracavity field amplitude, and the input noise of the probe cavity mode. The presence of the probe mode affects the system dynamics, but if the driving of the probe mode is much weaker so that  $|\alpha_p| \ll |\alpha_s|$ , the back-action of the probe mode on the resonator can be neglected. If one chooses parameters so that  $\Delta_p = \omega_m \gg k_p, G_p|\alpha_p|$ , one can rewrite Eq. (57) in the frame rotating at  $\Delta_p = \omega_m$  for the slow variables  $\delta\tilde{o}(t) \equiv \delta o(t) \exp\{i\omega_m t\}$  and neglect fast oscillating terms, so to get

$$\delta\dot{\tilde{a}}_p = -\kappa_p\delta\tilde{a}_p + i\frac{G_p\alpha_p}{\sqrt{2}}\delta\tilde{b} + \sqrt{2\kappa_p}\tilde{a}_p^{in}(t), \quad (58)$$

where  $\delta b = (i\delta p + \delta q)/\sqrt{2}$  is the mechanical annihilation operator. Finally, if  $\kappa_p \gg G_p|\alpha_p|/\sqrt{2}$ , the probe mode adiabatically follows the resonator dynamics and one has

$$\delta\tilde{a}_p \simeq i\frac{G_p\alpha_p}{\kappa_p\sqrt{2}}\delta\tilde{b} + \sqrt{\frac{2}{\kappa_p}}\tilde{a}_p^{in}(t). \quad (59)$$

The input-output relation  $\tilde{a}_p^{out} = \sqrt{2\kappa_p}\delta\tilde{a}_p - \tilde{a}_p^{in}$  [79] implies

$$\tilde{a}_p^{out} = i\frac{G_p\alpha_p}{\sqrt{\kappa_p}}\delta\tilde{b} + \tilde{a}_p^{in}(t), \quad (60)$$

showing that, in the chosen parameter regime, the output light of the probe mode gives a direct measurement of the resonator dynamics. With an appropriate calibration and applying standard quantum tomographic techniques

[89] to this output field, one can therefore reconstruct the quantum state of the resonator.

An alternative way to detect the resonator state by means of state transfer onto an optical mode, which does not require an additional probe mode, can be devised by appropriately exploiting the strong coupling regime. In this second example state transfer is realized in a transient regime soon after the preparation of the desired resonator state. One sets the cavity onto resonance  $\Delta = 0$  so that the system is always stable, and then strongly increases the input power in order to make the coupling  $G$  very large,  $G \gg \kappa, n_0\gamma_m$ . Under these conditions, coherent evolution driven by radiation pressure dominates and one has state swapping from the mechanical resonator onto the intracavity mode in a time  $t_{swap} \simeq \pi/2G$  so that the cavity mode reproduces the resonator state with a fidelity very close to unity. The fidelity of the swap can be computed and reads

$$F = \left[ \sqrt{\det(\mathcal{V}_1 + \mathcal{V}_2) + (\det \mathcal{V}_1 - 1/4)(\det \mathcal{V}_2 - 1/4)} - \sqrt{(\det \mathcal{V}_1 - 1/4)(\det \mathcal{V}_2 - 1/4)} \right]^{-1}, \quad (61)$$

where  $\mathcal{V}_1, \mathcal{V}_2$  are the block matrices in Eq. (32). The resulting fidelity under realistic conditions is plotted in Fig. (5d) as a function of  $G/\omega_m$  for  $\kappa/\omega_m = 0.2, 0.5, 1$  and  $2$ . One can see that the fidelity is close to unity around the optimal cooling regime and that in this regime *both the mechanical resonator and intracavity field thermalize in the same state*. Under this condition one can reconstruct the quantum state of the mechanical mode from the detection of the cavity output.

#### 4 Entanglement generation with a single driven cavity mode

As discussed in the introduction, a cavity coupled to a mechanical degree of freedom is capable of producing entanglement between the mechanical and the optical modes and also purely optical entanglement between the induced motional sidebands. In the following we elucidate the physical origins of this entanglement and analyze its magnitude and temperature robustness. Moreover, we analyze its use as a quantum-communication network resource in which the mechanical modes play the role of local nodes that store quantum information and optical modes carry this information among nodes. To this purpose we apply a multiplexing approach that allows one, by means of spectral filters, to select many traveling output modes originating from a single intracavity field.

#### 4.1 Intracavity optomechanical entanglement

Entanglement can be easily evaluated and quantified using the logarithmic negativity of Eq. (31), which requires the knowledge of the CM of the system of interest. For the steady state of the intracavity field-resonator system, the CM is determined in a straightforward way by the solution of Eq. (29). However, before discussing the general result we try to give an intuitive idea of how robust optomechanical entanglement can be generated, by using the sideband picture. Using the mechanical annihilation operator  $\delta b$  introduced in the above section, the linearized QLE of Eqs. (15)-(18) can be rewritten as

$$\begin{aligned}\dot{\delta\tilde{b}} &= -\frac{\gamma_m}{2} (\delta\tilde{b} - \delta\tilde{b}^\dagger e^{2i\omega_m t}) + \sqrt{\gamma_m} b^{in} + i\frac{G}{2} (\delta\tilde{a}^\dagger e^{i(\Delta+\omega_m)t} + \delta\tilde{a} e^{i(\omega_m-\Delta)t}) \\ \dot{\delta\tilde{a}} &= -\kappa\delta\tilde{a} + i\frac{G}{2} (\delta\tilde{b}^\dagger e^{i(\Delta+\omega_m)t} + \delta\tilde{b} e^{i(\Delta-\omega_m)t}) + \sqrt{2\kappa}\tilde{a}^{in}.\end{aligned}\quad (63)$$

We have introduced the tilded slowly evolving operators  $\delta\tilde{b}(t) = \delta b(t)e^{i\omega_m t}$ ,  $\delta\tilde{a}(t) = \delta a(t)e^{i\Delta t}$ , and the noises  $\tilde{a}^{in}(t) = a^{in}(t)e^{i\Delta t}$  and  $b^{in}(t) = \xi(t)e^{i\omega_m t}/\sqrt{2}$ . The input noise  $\tilde{a}^{in}(t)$  possesses the same correlation function as  $a^{in}(t)$ , while the Brownian noise  $b^{in}(t)$  in the limit of large mechanical frequency  $\omega_m$  acquires ‘‘optical-like’’ correlation functions  $\langle b^{in,\dagger}(t)b^{in}(t') \rangle = n_0\delta(t-t')$  and  $\langle b^{in}(t)b^{in,\dagger}(t') \rangle = [n_0 + 1]\delta(t-t')$  [90]. Eqs. (62)-(63) show that the cavity mode and mechanical resonator are coupled by radiation pressure via two kinds of interactions: i) a down-conversion process with interaction Hamiltonian  $\delta\tilde{b}^\dagger\delta\tilde{a}^\dagger + \delta\tilde{a}\delta\tilde{b}$ , which is modulated by a factor oscillating at  $\omega_m + \Delta$ ; ii) a beam-splitter-like process with interaction Hamiltonian  $\delta\tilde{b}^\dagger\delta\tilde{a} + \delta\tilde{a}^\dagger\delta\tilde{b}$ , modulated by a factor oscillating at  $\omega_m - \Delta$ . Therefore, by tuning the cavity into resonance with either the Stokes sideband of the driving laser,  $\Delta = -\omega_m$ , or the anti-Stokes sideband of the driving laser,  $\Delta = \omega_m$ , one can resonantly enhance one of the two processes. In the rotating wave approximation (RWA), which is justified in the limit of  $\omega_m \gg G, \kappa$ , the off-resonant interaction oscillates very fast with respect to the timescales of interest and can be neglected. Therefore, in the RWA regime, when one chooses  $\Delta = -\omega_m$ , the radiation pressure induces a down-conversion process, which is known to generate bipartite CV entanglement. Instead when one chooses  $\Delta = \omega_m$ , the dominant process is the beam-splitter-like interaction, which is not able to generate optomechanical entanglement starting from classical input states [91], as in this case. This argument leads to the conclusion that, in the RWA limit  $\omega_m \gg G, \kappa$ , the best regime for optomechanical entanglement is when the laser is blue-detuned from the cavity resonance  $\Delta = -\omega_m$  and down-conversion is enhanced. However, this argument is valid only in the RWA limit and it is strongly limited by the stability conditions, which rather force to work in the opposite regime of a red-detuned laser. In fact, the stability condition of Eq. (20) in the RWA limit  $\Delta = -\omega_m \gg \kappa, \gamma_m$ , simplifies to  $G < \sqrt{2\kappa\gamma_m}$ . Since one needs small mechani-

cal dissipation rate  $\gamma_m$  in order to see quantum effects, this means a very low maximum value for  $G$ . The logarithmic negativity  $E_{\mathcal{N}}$  is an increasing function of the effective optomechanical coupling  $G$  (as expected) and therefore the stability condition puts a strong upper bound also on  $E_{\mathcal{N}}$ . It is possible to prove that the following bound on  $E_{\mathcal{N}}$  exists [69]

$$E_{\mathcal{N}} \leq \ln \left[ \frac{1 + G/\sqrt{2\kappa\gamma_m}}{1 + n_0} \right], \quad (64)$$

showing that  $E_{\mathcal{N}} \leq \ln 2$  and above all that entanglement is extremely fragile with respect to temperature in the blue-detuned case because, due to the stability constraints,  $E_{\mathcal{N}}$  vanishes as soon as  $n_0 \geq 1$ .

This suggests that, due to instability, one can find significant intracavity optomechanical entanglement, which is also robust against temperature, only far from the RWA regime, in the strong coupling regime in the region with positive  $\Delta$ , because Eq. (22) allows for higher values of the coupling ( $G < \sqrt{\kappa^2 + \omega_m^2}$  when  $\Delta = \omega_m$ ). This is confirmed by Fig. 6a, where the *exact*  $E_{\mathcal{N}}$  calculated from the solution of Eq. (29) is plotted versus the normalized detuning  $\Delta/\omega_m$  and the normalized effective optomechanical coupling  $G/\omega_m$ . One sees that  $E_{\mathcal{N}}$  reaches significant values close to the bistability threshold; moreover it is possible to see that such intracavity entanglement is robust against thermal noise because it survives up to reservoir temperatures around 20 K [64]. It is also interesting to compare the conditions for optimal entanglement and cooling in this regime where the cavity is resonant with the anti-Stokes sideband. In Fig. 6b,  $n$  is plotted versus the same variables in the same parameter region. One can see that, while good entanglement is accompanied by good cooling, optimal entanglement is achieved for the largest possible coupling  $G$  allowed by the stability condition. This condition is far from the optimal cooling regime, which does not require very large  $G$  because otherwise the radiation pressure noise contribution and consequently the position variance become too large (see Eq. (54) and Fig. 5) [69].

#### 4.2 Entanglement with output modes

Let us now define and evaluate the entanglement of the mechanical resonator with the fields at the cavity output, which may represent an essential tool for the future integration of micromechanical resonators as quantum memories within quantum information networks. The intracavity field  $\delta a(t)$  and its output are related by the usual input-output relation [79]

$$a^{out}(t) = \sqrt{2\kappa}\delta a(t) - a^{in}(t), \quad (65)$$

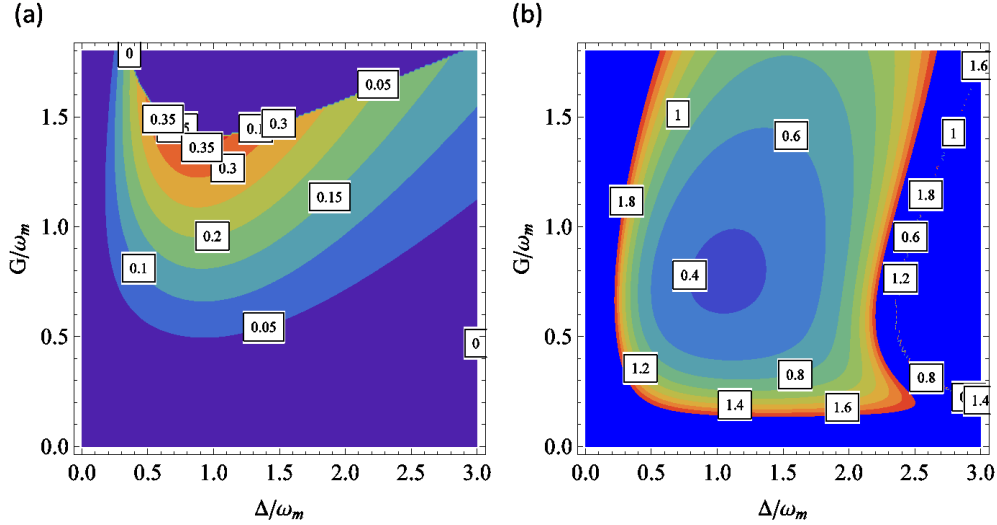


Fig. 6. Intracavity entanglement and cooling in the red-detuned regime. (a) Contour plot of logarithmic negativity of the field-mirror system at the steady state as a function of  $G/\omega_m$  and  $\Delta/\omega_m$  for the parameters  $p_0$  and  $\kappa = \omega_m$ . (b)  $n$  in the same parameter region: the plot shows that optimal cooling and optimal entanglement are both achieved close to  $\Delta/\omega_m \simeq 1$ . However, optimal cooling is obtained for smaller values of  $G/\omega_m$  with respect to entanglement.

where the output field possesses the same correlation functions of the optical input field  $a^{in}(t)$  and the same commutation relation, i.e., the only nonzero commutator is  $[a^{out}(t), a^{out}(t')^\dagger] = \delta(t - t')$ . From the continuous output field  $a^{out}(t)$  one can extract many independent optical modes, by selecting different time intervals or equivalently, different frequency intervals (see e.g. [92]). One can define a generic set of  $N$  output modes by means of the corresponding annihilation operators

$$a_k^{out}(t) = \int_{-\infty}^t ds g_k(t-s) a^{out}(s), \quad k = 1, \dots, N, \quad (66)$$

where  $g_k(s)$  is the causal filter function defining the  $k$ -th output mode. These annihilation operators describe  $N$  independent optical modes when  $[a_j^{out}(t), a_k^{out}(t)^\dagger] = \delta_{jk}$ , which is verified when

$$\int_0^\infty ds g_j(s)^* g_k(s) = \delta_{jk}, \quad (67)$$

i.e., the  $N$  filter functions  $g_k(t)$  form an orthonormal set of square-integrable functions in  $[0, \infty)$ . The situation can be equivalently described in the frequency domain: taking the Fourier transform of Eq. (66), one has

$$\tilde{a}_k^{out}(\omega) = \int_{-\infty}^\infty \frac{dt}{\sqrt{2\pi}} a_k^{out}(t) e^{i\omega t} = \sqrt{2\pi} \tilde{g}_k(\omega) a^{out}(\omega), \quad (68)$$



where  $\tilde{g}_k(\omega)$  is the Fourier transform of the filter function. An explicit example of an orthonormal set of filter functions is given by

$$g_k(t) = \frac{\theta(t) - \theta(t - \tau)}{\sqrt{\tau}} e^{-i\Omega_k t}, \quad (69)$$

( $\theta$  denotes the Heavyside step function) provided that  $\Omega_k$  and  $\tau$  satisfy the condition

$$\Omega_j - \Omega_k = \frac{2\pi}{\tau} p, \quad \text{integer } p. \quad (70)$$

These functions describe a set of independent optical modes, each centered around the frequency  $\Omega_k$  and with time duration  $\tau$ , i.e., frequency bandwidth  $\sim 1/\tau$ , since

$$\tilde{g}_k(\omega) = \sqrt{\frac{\tau}{2\pi}} e^{i(\omega - \Omega_k)\tau/2} \frac{\sin [(\omega - \Omega_k)\tau/2]}{(\omega - \Omega_k)\tau/2}. \quad (71)$$

When the central frequencies differ by an integer multiple of  $2\pi/\tau$ , the corresponding modes are independent due to the destructive interference of the oscillating parts of the spectrum.

The entanglement between the output modes defined above and the mechanical mode is fully determined by the corresponding  $(2N + 2) \times (2N + 2)$  CM, which is defined by

$$\mathcal{V}_{ij}^{out}(t) = \frac{1}{2} \langle u_i^{out}(t) u_j^{out}(t) + u_j^{out}(t) u_i^{out}(t) \rangle, \quad (72)$$

where

$$u^{out}(t) = \left( \delta q(t), \delta p(t), X_1^{out}(t), Y_1^{out}(t), \dots, X_N^{out}(t), Y_N^{out}(t) \right)^T \quad (73)$$

is the vector formed by the mechanical position and momentum fluctuations and by the amplitude ( $X_k^{out}(t) = [a_k^{out}(t) + a_k^{out}(t)^\dagger] / \sqrt{2}$ ), and phase ( $Y_k^{out}(t) = [a_k^{out}(t) - a_k^{out}(t)^\dagger] / i\sqrt{2}$ ) quadratures of the  $N$  output modes. The vector  $u^{out}(t)$  properly describes  $N + 1$  independent CV bosonic modes, and in particular the mechanical resonator is independent of (i.e., it commutes with) the  $N$  optical output modes because the latter depend upon the output field at former times only ( $s < t$ ). From the intracavity CM and Eqs. (65),(66), and (72) one can determine the  $(N + 1) \times (N + 1)$  CM matrix  $\mathcal{V}^{out}$  at the steady state [69].

Let us first consider the case when we select and detect only one mode at the cavity output. Just to fix the ideas, we choose the mode specified by the filter function of Eqs. (69) and (71), with central frequency  $\Omega$  and bandwidth  $\tau^{-1}$ . Straightforward choices for this output mode are a mode centered either at the cavity frequency,  $\Omega = \omega_c - \omega_l$ , or at the driving laser frequency,  $\Omega = 0$  (we are in the rotating frame and therefore all frequencies are referred to the laser frequency  $\omega_l$ ), and with a bandwidth of the order of the cavity bandwidth

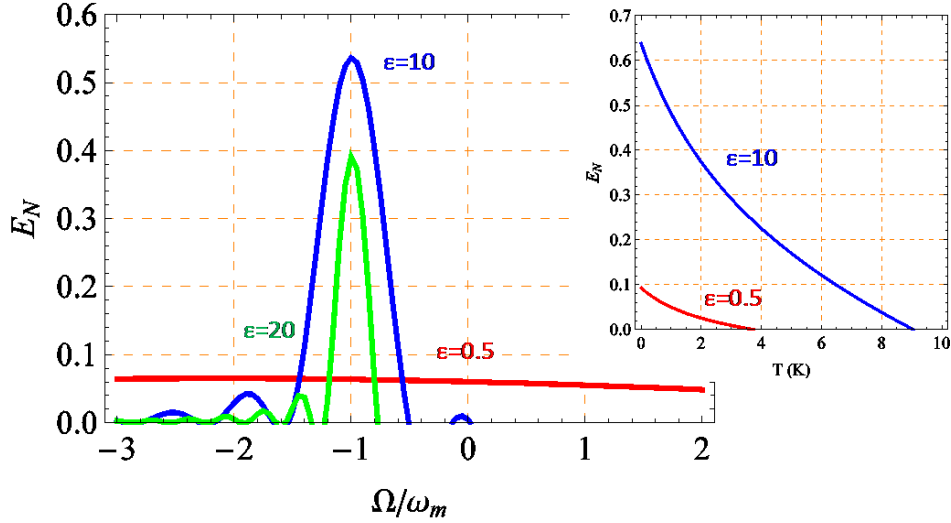


Fig. 7. Resonator-output field entanglement when the central frequency of the output mode is swept around the laser frequency. Parameters are  $p_0$ ,  $\Delta = \omega_m$ ,  $G = \omega_m/2$  and  $\kappa = \omega_m$ . The entanglement is optimized when the output mode coincides with the Stokes sideband of the laser ( $\Omega = -\omega_m$ ), with the appropriate bandwidth ( $\epsilon \simeq 10$ , corresponding to  $\tau\gamma_m^{eff} \simeq 1$ ). For smaller  $\epsilon$ , the selected output mode mixes Stokes and anti-Stokes photons and the entanglement is weak, while for larger  $\epsilon$  only a fraction of the sideband is selected and part of the quantum correlations are lost. In the inset the robustness of Stokes-mirror  $E_N$  with respect to temperature is shown.

$\tau^{-1} \simeq \kappa$ . However, as discussed above, the motion of the mechanical resonator generates Stokes and anti-Stokes motional sidebands, consequently modifying the cavity output spectrum.

In order to determine the output optical mode which is better entangled with the mechanical resonator, we study the logarithmic negativity  $E_N$  associated with the output CM  $\mathcal{V}^{out}$  (for  $N = 1$ ) as a function of the central frequency of the mode  $\Omega$  and its bandwidth  $\tau^{-1}$ , at the same parameter region considered in the previous subsection,  $p_0$  and  $\Delta = \omega_m$ , where intracavity entanglement is optimal. The results are shown in Fig. 7, where  $E_N$  is plotted versus  $\Omega/\omega_m$  at different values of  $\epsilon = \tau\omega_m$ . If  $\epsilon \lesssim 1$ , i.e., the bandwidth of the detected mode is larger than  $\omega_m$ , the detector does not resolve the motional sidebands, and  $E_N$  has a value (roughly equal to that of the intracavity case) which does not essentially depend upon the central frequency. For smaller bandwidths (larger  $\epsilon$ ), the sidebands are resolved by the detection and the role of the central frequency becomes important. In particular  $E_N$  becomes highly peaked around the *Stokes sideband*  $\Omega = -\omega_m$ , showing that the optomechanical entanglement generated within the cavity is mostly carried by this lower frequency sideband. What is relevant is that the optomechanical entanglement of the output mode is significantly larger than its intracavity counterpart and achieves its maximum value at the optimal value  $\epsilon \simeq 10$ , i.e., a detection band-

width  $\tau^{-1} \simeq \omega_m/10$ . This means that in practice, by appropriately filtering the output light, one realizes an *effective entanglement distillation* because the selected output mode is more entangled with the mechanical resonator than the intracavity field.

The fact that the output mode which is most entangled with the mechanical resonator is the one centered around the Stokes sideband is also consistent with the physics of a previous model analyzed in [66]. In [66], a free-space optomechanical model is discussed, where the entanglement between a vibrational mode of a perfectly reflecting micro-mirror and the two first motional sidebands of an intense laser beam shined on the mirror is analyzed. Also in that case, the mechanical mode is entangled only with the Stokes mode and it is not entangled with the anti-Stokes sideband.

One can also understand why the output mode optimally entangled with the mechanical mode has a finite bandwidth  $\tau^{-1} \simeq \omega_m/10$  (for the chosen operating point). In fact, the optimal situation is achieved when the detected output mode overlaps as best as possible with the Stokes peak in the spectrum, and therefore  $\tau^{-1}$  coincides with the width of the Stokes peak. This width is determined by the effective damping rate of the mechanical resonator,  $\gamma_m^{eff} = \gamma_m + \Gamma$ , given by the sum of the intrinsic damping rate  $\gamma_m$  and the net laser cooling rate  $\Gamma$  of Eq. (52). It is possible to check that, with the chosen parameter values, the condition  $\varepsilon = 10$  corresponds to  $\tau^{-1} \simeq \gamma_m^{eff}$ .

It is finally important to analyze the robustness of the present optomechanical entanglement with respect to temperature. As discussed above and shown in [64], the entanglement of the resonator with the intracavity mode is very robust. It is important to see if this robustness is kept also by the optomechanical entanglement of the output mode. This is shown also in the inset of Fig. 7, where the logarithmic negativity  $E_{\mathcal{N}}$  of the output mode centered at the Stokes sideband  $\Omega = -\omega_m$  is plotted versus the temperature of the reservoir at two different values of the bandwidth, the optimal one  $\varepsilon = 10$ , and at a larger bandwidth  $\varepsilon = 0.5$ . We see the expected decay of  $E_{\mathcal{N}}$  for increasing temperature, but above all that also this output optomechanical entanglement is robust against temperature because it persists even above liquid He temperatures, at least in the case of the optimal detection bandwidth  $\varepsilon = 10$ .

### 4.3 Optical entanglement between sidebands

Let us now consider the case where we detect at the output two independent, well resolved, optical output modes. We use again the step-like filter functions of Eqs. (69) and (71), assuming the same bandwidth  $\tau^{-1}$  for both modes and two different central frequencies,  $\Omega_1$  and  $\Omega_2$ , satisfying the orthogonality

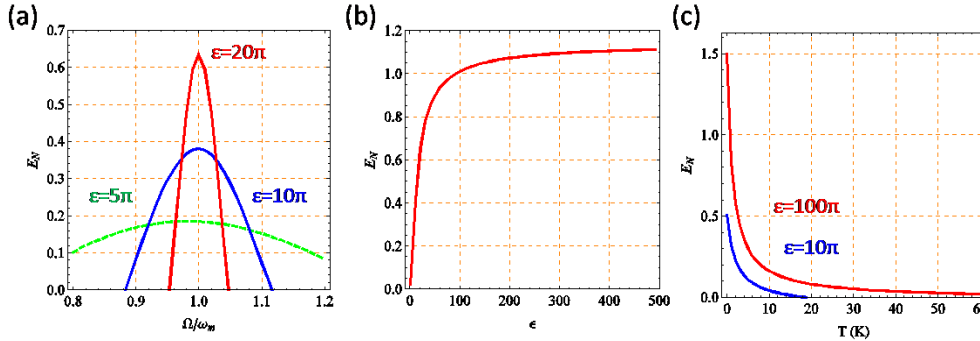


Fig. 8. Sideband-sideband entanglement. Parameters  $p_0$ ,  $\kappa = \omega_m$  and  $G = \omega_m/2$ . (a) Assuming one detection setup centered at the Stokes sideband and sweeping the second detection frequency around the anti-Stokes sideband at  $\Omega = \omega_m$ , the entanglement is clearly shown to be optimized when the anti-Stokes output field is detected. This entanglement is improving with smaller and smaller detection bandwidth ( $\epsilon \rightarrow \infty$ ). (b) Logarithmic negativity increases asymptotically to a finite value with  $\epsilon \rightarrow \infty$ . (c) Temperature robustness for  $\epsilon = 10\pi$  and  $\epsilon = 100\pi$ . The entanglement survives to very high temperatures.

condition of Eq. (70)  $\Omega_1 - \Omega_2 = 2p\pi\tau^{-1}$  for some integer  $p$ , in order to have two independent optical modes. It is interesting to analyze the stationary state of the resulting tripartite CV system formed by the two output modes and the mechanical mode, in order to see if and when it is able to show purely optical bipartite entanglement between the two output modes.

The generation of two entangled light beams by means of the radiation pressure interaction of these fields with a mechanical element has been already considered in various configurations. In Ref. [93], and more recently in Ref. [63], two modes of a Fabry-Perot cavity system with a movable mirror, each driven by an intense laser, are entangled at the output due to their common ponderomotive interaction with the movable mirror (the scheme has been then generalized to many driven modes in [94]). In the single mirror free-space model of Ref. [66], the two first motional sidebands are also robustly entangled by the radiation pressure interaction as in a two-mode squeezed state produced by a non-degenerate parametric amplifier [95]. Robust two-mode squeezing of a bimodal cavity system can be similarly produced if the movable mirror is replaced by a single ion trapped within the cavity [96].

The situation considered here is significantly different from that of Refs. [63,93,94,96], which require many driven cavity modes, each associated with the corresponding output mode. In the present case instead, the different output modes *originate from the same single driven cavity mode*, and therefore it is simpler from an experimental point of view. The present scheme can be considered as a sort of “cavity version” of the free-space case of Ref. [66], where the reflecting mirror is driven by a single intense laser. Therefore, as in [66,95], one expects to find a parameter region where the two output modes centered

around the two motional sidebands of the laser are entangled. This expectation is clearly confirmed by Fig. 8a, where the logarithmic negativity  $E_{\mathcal{N}}$  associated with the bipartite system formed by the output mode centered at the Stokes sideband ( $\Omega_1 = -\omega_m$ ) and a second output mode with the same inverse bandwidth ( $\varepsilon = \omega_m\tau = 10\pi$ ) and a variable central frequency  $\Omega$ , is plotted versus  $\Omega/\omega_m$ .  $E_{\mathcal{N}}$  is calculated from the CM  $\mathcal{V}^{out}$  (for  $N = 2$ ) eliminating the first two rows associated with the mechanical mode. One can clearly see that bipartite entanglement between the two cavity outputs exists only in a narrow frequency interval around the anti-Stokes sideband,  $\Omega = \omega_m$ , where  $E_{\mathcal{N}}$  achieves its maximum. This shows that, as in [66,95], the two cavity output modes corresponding to the Stokes and anti-Stokes sidebands of the driving laser are significantly entangled by their common interaction with the mechanical resonator. The advantage of the present cavity scheme with respect to the free-space case of [66,95] is that the parameter regime for reaching radiation-pressure mediated optical entanglement is much more promising from an experimental point of view because it requires less input power and a not too large mechanical quality factor of the resonator. In Fig. 8b, the dependence of  $E_{\mathcal{N}}$  of the two output modes centered at the two sidebands  $\Omega = \pm\omega_m$  upon their inverse bandwidth  $\varepsilon$  is studied. We see that, differently from optomechanical entanglement of the former subsection, the logarithmic negativity of the two sidebands always increases for decreasing bandwidth, and it achieves a significant value, comparable to that achievable with parametric oscillators, for very narrow bandwidths. This fact can be understood from the fact that quantum correlations between the two sidebands are established by the coherent scattering of the cavity photons by the oscillator, and that the quantum coherence between the two scattering processes is maximal for output photons with frequencies  $\omega_l \pm \omega_m$ . Figs. 7 and 8 show that in the chosen parameter regime, the output mode centered around the Stokes sideband mode shows bipartite entanglement simultaneously with the mechanical mode and with the anti-Stokes sideband mode. This fact suggests that the CV tripartite system formed by the output Stokes and anti-Stokes sidebands and the mechanical resonator mode might be characterized by a fully tripartite-entangled stationary state. This is actually true and it can be checked by applying the classification criterion of Ref. [97], providing a necessary and sufficient criterion for the determination of the entanglement class in the case of tripartite CV Gaussian states, which is directly computable in terms of the eigenvalues of appropriate test matrices [97] (see Ref. [69]).

## 5 Entanglement generation with two driven cavity modes

We now generalize the system by considering the case when *two* cavity modes with different frequencies are intensely driven. We shall focus onto a param-

eter regime which will prove to be convenient for the generation of robust stationary CV entanglement between the resonator and the two cavity modes. A bichromatic driving of a cavity has been already experimentally considered in Refs. [21]. There however it was employed for cooling a macroscopically heavy ( $m \simeq 1g$ ) movable mirror. One driven mode is used to “trap” the mirror, i.e., to induce a strong optical spring effect increasing by three orders of magnitude the oscillation frequency. The other driven mode is instead used to cool the mechanical resonator by increasing the effective mechanical damping, either via back-action, or via cold-damping feedback. The bichromatic driving configuration has been already considered for the generation of entanglement in various configurations in some theoretical proposals. In fact, in Ref. [93], and more recently in Ref. [63], two modes of a Fabry-Perot cavity system, each driven by an intense laser, are entangled at the output due to their common ponderomotive interaction with the movable mirror.

### 5.1 Quantum Langevin equations and stability conditions

We generalize the Hamiltonian of Eq. (1) by considering *two* cavity modes, with frequencies  $\omega_{cA}$  and  $\omega_{cB}$ , each driven by a laser with frequency  $\omega_{0A}$  and  $\omega_{0B}$ , and power  $\mathcal{P}_A$  and  $\mathcal{P}_B$ , respectively. The resulting Hamiltonian is

$$H = \hbar\omega_{cA} a^\dagger a + \hbar\omega_{cB} b^\dagger b + \frac{1}{2}\hbar\omega_m(p^2 + q^2) - \hbar(G_{0A} a^\dagger a + G_{0B} b^\dagger b)q + i\hbar[E_A(a^\dagger e^{-i\omega_{0A}t} - a e^{i\omega_{0A}t}) + E_B(b^\dagger e^{-i\omega_{0B}t} - b e^{i\omega_{0B}t})], \quad (74)$$

where  $a$  and  $b$  now denote the annihilation operators of the two cavity modes, we have introduced the two coupling constants  $G_{0x} = \sqrt{\hbar/m\omega_m\omega_{cx}}/L$ , and the two driving rates  $|E_x| = \sqrt{2P_x\kappa/\hbar\omega_{0x}}$ ,  $x = A, B$ . We have assumed for simplicity that the two modes have the same decay rate  $\kappa$ . We assume that scattering of photons of the driven modes into other cavity modes and also between the two chosen modes is negligible: this is verified when  $\omega_m$  is much smaller than the free spectral range of the cavity.

Introducing again dissipation and noise terms as in Sec. 2, the system dynamics is described by the following set of nonlinear QLE, written in the interaction picture with respect to  $\hbar\omega_{0A}a^\dagger a + \hbar\omega_{0B}b^\dagger b$ ,

$$\dot{q} = \omega_m p, \quad (75)$$

$$\dot{p} = -\omega_m q - \gamma_m p + G_{0A} a^\dagger a + G_{0B} b^\dagger b + \xi, \quad (76)$$

$$\dot{a} = -[\kappa + i(\Delta_{0A} - G_{0A}q)]a + E_A + \sqrt{2\kappa}a^{in}, \quad (77)$$

$$\dot{b} = -[\kappa + i(\Delta_{0B} - G_{0B}q)]b + E_B + \sqrt{2\kappa}b^{in}, \quad (78)$$

where  $\Delta_{0x} \equiv \omega_{cx} - \omega_{0x}$  are the detunings of the two lasers, and we have introduced a vacuum input noise  $b^{in}(t)$  for the cavity mode  $b$ , possessing the same correlations of Eqs. (7)-(8).

We assume again that both modes are intensely driven so that the system is characterized by a semiclassical steady state with large intracavity amplitudes for both modes and a modified cavity length. This classical steady state is determined by setting the time derivatives to zero, factorizing the averages and solving for the mean values  $a_s = \langle a \rangle$ ,  $b_s = \langle b \rangle$ ,  $q_s = \langle q \rangle$ ,  $p_s = \langle p \rangle$ . One gets

$$a_s = \frac{E_A}{\kappa + i\Delta_A}, \quad (79)$$

$$b_s = \frac{E_B}{\kappa + i\Delta_B}, \quad (80)$$

$$q_s = \frac{G_{0A}|a_s|^2 + G_{0B}|b_s|^2}{\omega_m}, \quad (81)$$

$$p_s = 0, \quad (82)$$

where the effective detunings  $\Delta_x \equiv \Delta_{0x} - (G_{0A}^2|a_s|^2 + G_{0B}^2|b_s|^2)/\omega_m$ ,  $x = A, B$ , have been defined, so that Eqs. (79)-(80) form actually a system of nonlinear equations, whose solution gives the stationary amplitudes  $a_s$  and  $b_s$ .

One then focuses onto the dynamics of the quantum fluctuations around this steady state, which are well described by linearizing the QLE of Eqs. (75)-(78) around the semiclassical steady state values, provided that  $|a_s|, |b_s| \gg 1$ . The linearized QLE for the resonator and for the amplitude and phase quadratures of the two modes,  $\delta X_A$ ,  $\delta X_B$ ,  $\delta Y_A$  and  $\delta Y_B$ , defined as in Sec. 2, can be written in compact form as

$$\dot{u}(t) = Au(t) + n(t),$$

where  $u = (\delta q, \delta p, \delta X_A, \delta Y_A, \delta X_B, \delta Y_B)^T$  is the vector of quadrature fluctuations, and  $n = (0, \xi, \sqrt{2\kappa}X_A^{in}, \sqrt{2\kappa}Y_A^{in}, \sqrt{2\kappa}X_B^{in}, \sqrt{2\kappa}Y_B^{in})^T$  is the corresponding vector of noises. The  $6 \times 6$  matrix  $A$  is the drift matrix of the system, which reads

$$A = \begin{pmatrix} 0 & \omega_m & 0 & 0 & 0 & 0 \\ -\omega_m & \gamma_m & G_A & 0 & G_B & 0 \\ 0 & 0 & -\kappa & \Delta_A & 0 & 0 \\ G_A & 0 & -\Delta_A & -\kappa & 0 & 0 \\ 0 & 0 & 0 & 0 & -\kappa & \Delta_B \\ G_B & 0 & 0 & 0 & -\Delta_B & -\kappa \end{pmatrix}, \quad (83)$$

where we have chosen the phase reference of the two cavity modes so that  $a_s$

and  $b_s$  are real and positive, and defined the effective couplings  $G_A = G_{0A}a_s\sqrt{2}$  and  $G_B = G_{0B}b_s\sqrt{2}$ .

The steady state exists and it is stable if all the eigenvalues of the drift matrix  $A$  have negative real parts. The parameter region under which stability is verified can be obtained from the Routh-Hurwitz criteria [81], but the inequalities that come out in the present case are quite involved. One can have an idea of this fact from the expression of the characteristic polynomial of  $A$ ,  $P(\lambda) = \lambda^6 + c_1\lambda^5 + c_2\lambda^4 + c_3\lambda^3 + c_4\lambda^2 + c_5\lambda + c_6$ , where

$$\begin{aligned}
c_1 &= \gamma_m + 4\kappa, \\
c_2 &= \Delta_A^2 + \Delta_B^2 + 4\gamma_m\kappa + 6\kappa^2 + \omega_m^2, \\
c_3 &= \gamma_m(\Delta_A^2 + \Delta_B^2 + 6\kappa^2) + 2\kappa[\Delta_A^2 + \Delta_B^2 + 2(\kappa^2 + \Omega_m^2)], \\
c_4 &= \kappa^4 + 2\gamma_m\kappa(\Delta_B^2 + 2\kappa^2) + 6\kappa^2\omega_m^2 + \Delta_B^2(\kappa^2 + \omega_m^2) + \\
&\quad \Delta_A^2(\Delta_B^2 + 2\gamma_m\kappa + \kappa^2 + \omega_m^2) - \omega_m(G_A^2\Delta_A + G_B^2\Delta_B), \\
c_5 &= \gamma_m(\Delta_A^2 + \kappa^2)(\Delta_B^2 + \kappa^2) + 2\kappa\omega_m^2(\Delta_A^2 + \Delta^2 + 2\kappa^2) \\
&\quad - 2\kappa\omega_m(G_A^2\Delta_A + G_B^2\Delta_B), \\
c_6 &= \omega_m^2(\Delta_A^2 + \kappa^2)(\Delta_B^2 + \kappa^2) - \omega_m[G_B^2\Delta_B(\Delta_A^2 + \kappa^2) \\
&\quad + G_A^2\Delta_A(\Delta_B^2 + \kappa^2)].
\end{aligned}$$

We are considering here a bichromatic driving of the cavity in order to improve the size and the robustness of the generated entanglement. Entanglement monotonically increases with the optomechanical coupling but, as we have seen also in the previous sections, the stability conditions put a strict upper bound on the maximum achievable value of this coupling. Therefore it is interesting to find a regime in which the presence of the second driven mode makes the system always stable, so that the couplings can be made very large (for example by increasing the input power, the cavity finesse, or decreasing the cavity length) without entering the unstable regime. One then hopes that in this regime also entanglement can be made large and robust against temperature.

A simple way to have always a stable system is to find a particular relation between the parameters such that the characteristic polynomial of  $A$  does not depend upon  $G_A$  and  $G_B$ . In this case, the eigenvalues of  $A$  would be independent of the two couplings and stability would be guaranteed. The expressions above show that the eigenvalues of  $A$  are independent of  $G_A$  and  $G_B$  and the system is always stable if and only if

$$|G_A| = |G_B| = G, \tag{84a}$$

$$\Delta_A = -\Delta_B = \Delta. \tag{84b}$$

The condition described by Eqs. (84) represents a perfect balance between a



cooling cavity mode (which, without loss of generality, we can take as mode  $A$ , so that  $\Delta_A > 0$ ) and a heating cavity mode, i.e., mode  $B$  with  $\Delta_B < 0$ . The fact that the eigenvalues of  $A$  do not depend upon the couplings means that the decay rates of both the resonator and the cavity modes are left unchanged and in this case radiation pressure mainly create quantum correlations, i.e., entanglement, between the modes. We shall assume conditions (84) from now on.

## 5.2 Entanglement of the output modes

We now calculate the entanglement properties of the steady state of the bichromatically driven cavity. However we shall not discuss here the intracavity entanglement, but only the entanglement properties of the optical *output modes*. In fact, as we have seen above in the case of a single driven mode, one can obtain a larger optomechanical entanglement with respect to the intracavity case by appropriately filtering the output modes. Moreover only the entanglement with output modes is relevant for any quantum communication application. We shall apply therefore the filter function formalism developed in Sec. 4.2, restricted however here to the simple case of *a single output mode* for each intracavity mode. In fact, we have now two driven cavity modes and considering the more general case of multiple output modes associated to each driven mode as in Sec. 4.2, would render the description much more involved without however gaining too much insight into the physics of the problem. The two output modes originate from two different cavity modes, and since the latter are not too close in frequency, they consequently describe two independent modes. Therefore we do not need orthogonal filter functions like those of Eq. (69) used for the single driven mode case, and we choose here a different filter function. We consider the two output modes with annihilation operators

$$a_{\Omega_x}^{out}(t) = \int_{-\infty}^t ds g_x(t-s) a_x^{out}(s) \quad x = A, B, \quad (85)$$

where  $a_A^{out}(t)$  and  $a_B^{out}(t)$  are the usual output fields associated with the two cavity modes and

$$g_x(t) = \sqrt{\frac{2}{\tau}} e^{-(1/\tau + i\Omega_x)t} \theta(t) \quad x = A, B \quad (86)$$

are the two filter functions, describing two output modes, both with bandwidth  $1/\tau$  and with central frequencies,  $\Omega_A$  and  $\Omega_B$ , which are in general different from the cavity mode frequencies  $\omega_{cA}$  and  $\omega_{cB}$ .

The entanglement between the chosen output modes and the mechanical resonator mode is fully determined by the corresponding  $6 \times 6$  CM, which is

defined as in Eq. (72)

$$\mathcal{V}_{ij}^{out}(t) = \frac{1}{2} \langle u_i^{out}(t) u_j^{out}(t) + u_j^{out}(t) u_i^{out}(t) \rangle, \quad (87)$$

where now

$$u^{out}(t) = [0, 0, \delta X_{\Omega_A}^{out}(t), \delta Y_{\Omega_A}^{out}(t), \delta X_{\Omega_B}^{out}(t), \delta Y_{\Omega_B}^{out}(t)]^T, \quad (88)$$

is the vector formed by the mechanical position and momentum fluctuations and by the amplitude and phase quadratures of the filtered modes. Using the various definitions, input-output relations and also the correlation function of the noise terms, one can derive an integral expression for the CM  $\mathcal{V}^{out}$  of the system (see Ref. [69] for the details in a similar calculation), which is given by

$$\mathcal{V}^{out} = \int d\omega \tilde{T}(\omega) \left[ \tilde{M}(\omega) + \frac{P_{out}}{2\kappa} \right] D(\omega) \left[ \tilde{M}(\omega)^\dagger + \frac{P_{out}}{2\kappa} \right] \tilde{T}(\omega)^\dagger, \quad (89)$$

where  $\tilde{T}(\omega)$  is the Fourier transform of

$$T(t) = \begin{pmatrix} \delta(t) & 0 & 0 & 0 & 0 & 0 \\ 0 & \delta(t) & 0 & 0 & 0 & 0 \\ 0 & 0 & \sqrt{2\kappa}\text{Reg}_A(t) & -\sqrt{2\kappa}\text{Im}g_A(t) & 0 & 0 \\ 0 & 0 & \sqrt{2\kappa}\text{Im}g_A(t) & \sqrt{2\kappa}\text{Reg}_A(t) & 0 & 0 \\ 0 & 0 & 0 & 0 & \sqrt{2\kappa}\text{Reg}_B(t) & -\sqrt{2\kappa}\text{Im}g_B(t) \\ 0 & 0 & 0 & 0 & \sqrt{2\kappa}\text{Im}g_B(t) & \sqrt{2\kappa}\text{Reg}_B(t) \end{pmatrix}, \quad (90)$$

$$\tilde{M}(\omega) = (i\omega + A)^{-1}, \quad (91)$$

$P_{out} = \text{Diag}[0, 0, 1, 1, 1, 1]$  is the projector onto the optical quadratures, and  $D(\omega)$  is the matrix associated with the Fourier transform of the noise correlation functions, given by

$$D(\omega) = \text{Diag}[0, (\gamma_m \omega / \omega_m) \coth(\hbar\omega / 2k_B T), \kappa, \kappa, \kappa, \kappa].$$

Using the CM  $\mathcal{V}^{out}$  one can analyze the entanglement between the three different bipartitions of the system, when one of the three modes is traced out, and also tripartite entanglement.

### 5.2.1 Optomechanical entanglement

First of all we consider the entanglement between the output field of the ‘‘cooling mode’’ (A) (the one with  $\Delta_A > 0$ ) and the mechanical resonator. We have seen in Sec. 4 that this configuration allows to achieve the maximum

optomechanical entanglement in the case of a single driven cavity mode. In fact, when  $\Delta \simeq \omega_m$ ,  $G$  is large enough, and the selected output mode is centered around the Stokes sideband, the entanglement is optimized and it is also robust against temperature (see Fig. 7). Fig. 9 shows that the presence of the second “heating” mode B *disturbs* this optimal condition and that  $E_{\mathcal{N}}$  is appreciably lower than the one with only one driven mode. In fact, we have considered here a similar parameter region, i.e.  $p_0, \kappa = \omega_m, \Delta_A = \omega_m, \Delta_B = -\omega_m, G_a = 0.326\omega_m, G_b = 0.302\omega_m$ . The qualitative behavior of  $E_{\mathcal{N}}$  is identical to that of the corresponding Fig. 7, i.e.,  $E_{\mathcal{N}}$  is maximum when the output mode overlaps as best as possible with the Stokes sideband of the corresponding driving laser, which means centered around  $-\omega_m$  and with an inverse bandwidth  $\varepsilon = \omega_m\tau \simeq 10$ . However the achievable values of  $E_{\mathcal{N}}$  are significantly *lower*. Fig. 7b shows that, despite the lower values, entanglement is still quite robust against temperature.

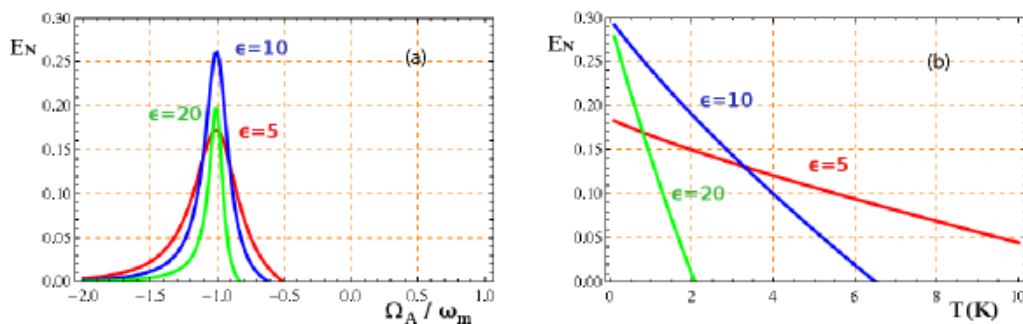


Fig. 9. Logarithmic negativity  $E_{\mathcal{N}}$  of the bipartite system formed by the mechanical mode and the output of the “cooling” mode A. (a)  $E_{\mathcal{N}}$  versus the center frequency of the output mode  $\Omega_A/\omega_m$  at three different values of the inverse detection bandwidth  $\varepsilon = \omega_m\tau$ . As in the single driven mode case (see Fig. 7), entanglement is maximum when the output mode is centered around the Stokes sideband  $\Omega_A = -\omega_m$ . The other parameters are  $p_0, \kappa = \omega_m, \Delta_A = \omega_m, \Delta_B = -\omega_m, G_a = 0.326\omega_m, G_b = 0.302\omega_m$ . (b)  $E_{\mathcal{N}}$  versus the reservoir temperature  $T$  when the output mode is centered at the Stokes sideband ( $\Omega_A = -\omega_m$ ) for the same three different values of  $\varepsilon$ .

The advantage of the bichromatic driving becomes instead apparent when one considers the bipartite system formed by the resonator and the output field of the “heating” mode (B), the one with  $\Delta_B = -\omega_m$ . The stationary optomechanical entanglement can achieve in this case significantly larger values. The results are shown in Fig. 10 which refers to the same parameters of Fig. 9 and shows the same qualitative behavior:  $E_{\mathcal{N}}$  is optimized when the selected output mode well overlaps with the Stokes sideband of the driving laser  $\Omega_B = -\omega_m$  and it persists up to reservoir temperatures of the order of 10 K. However,  $E_{\mathcal{N}}$  is now roughly three times larger than the corresponding value for the “cooling” mode. This behavior is different from what is found in Sec. 4 for a single driven cavity mode, where we have seen that optomechanical entanglement in the “heating” regime of negative detunings is seriously

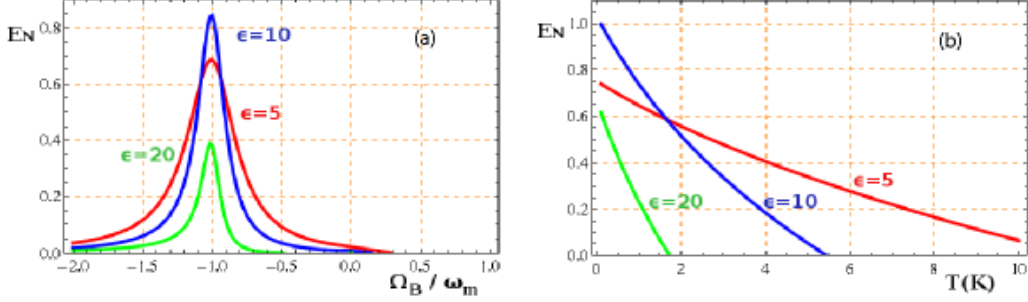


Fig. 10. Logarithmic negativity  $E_{\mathcal{N}}$  of the bipartite system formed by the mechanical mode and the output of the “heating” mode B. (a)  $E_{\mathcal{N}}$  versus the center frequency of the latter  $\Omega_A/\omega_m$  at three different values of the inverse detection bandwidth  $\epsilon = \omega_m\tau$ . As it happens for the “cooling” mode A, entanglement is maximum when the output mode is centered around the the Stokes sideband  $\Omega_B = -\omega_m$ . Parameters are as in Fig. 9. (b)  $E_{\mathcal{N}}$  versus the reservoir temperature  $T$  when the output mode is centered at the Stokes sideband ( $\Omega_B = -\omega_m$ ) for the same three different values of  $\epsilon$ .

limited by stability conditions. Now, thanks to the combined action of the two driven modes and to the conditions (84), the system is always stable and the parametric-like process described in Sec. 4 is able to generate large and robust entanglement. Therefore we can say that in this bichromatic case, mode A helps to entangle in a robust way the output of the “heating” mode B, by counteracting its instability effect and making the system stable for any value of the couplings  $G_A$  and  $G_B$ . Notice that in this case, the Stokes sideband of the laser driving mode B is *resonant* with the cavity, because  $\Delta_B = -\omega_m$  implies  $\omega_{cB} = \omega_{0B} - \omega_m = \omega_{Stokes}$  and this provides a further reason why the optomechanical entanglement may become large.

### 5.2.2 Purely optical entanglement between output modes

Let us consider now the purely optical entanglement between the two output light beams. As discussed at the beginning of the section, the possibility to entangle two different output modes of a cavity by means of radiation pressure has been already suggested in different configurations [63,66,93,95]. We have also seen in Sec. 4 that this is possible even with a single driven mode. It is nonetheless interesting to compare the results of Sec. 4 with the present bichromatic driving case. The bichromatic case has been already studied in Ref. [63], which however restricted to the case of output modes with infinitely narrow bandwidth ( $\tau = \infty$ ) and centered around the driving laser frequency ( $\Omega_A = \Omega_B = 0$ ). The general filter function formalism instead allows us to consider generic values of  $\tau$ ,  $\Omega_A$ , and  $\Omega_B$ . By applying again Eq. (89) and tracing out now the mechanical mode, we get the results illustrated in Fig. 11. We have considered a slightly different parameter regime with respect to the previous subsection, by choosing slightly larger couplings,  $G_a = 1.74\omega_m$ ,  $G_b = 1.70\omega_m$ ,

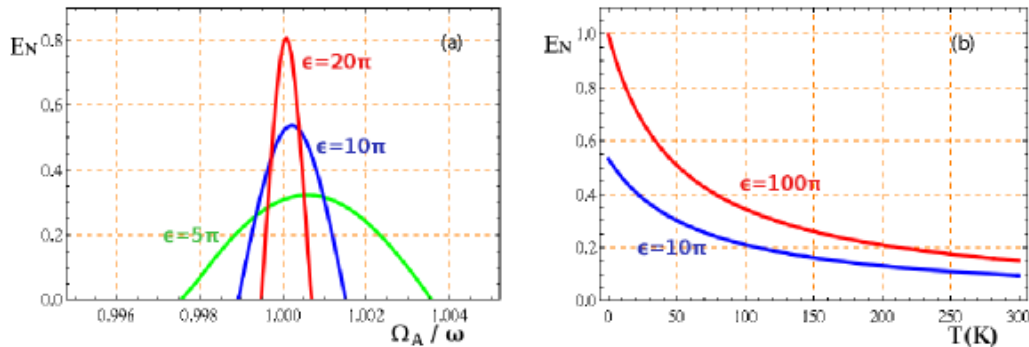


Fig. 11. Logarithmic negativity  $E_{\mathcal{N}}$  of the bipartite system formed by the output modes associated with the two driven cavity modes. (a)  $E_{\mathcal{N}}$  versus the center frequency of the “cooling” mode A  $\Omega_A/\omega_m$  for a center frequency of the “heating” mode fixed at  $\Omega_B = -\omega_m$  (Stokes sideband), and at three different values of the inverse detection bandwidth  $\epsilon = \omega_m\tau$ . The other parameters are  $p_0$ ,  $\kappa = \omega_m$ ,  $\Delta_A = \omega_m$ ,  $\Delta_B = -\omega_m$ ,  $G_a = 1.74\omega_m$ ,  $G_b = 1.70\omega_m$ . (b)  $E_{\mathcal{N}}$  versus the reservoir temperature  $T$  when the output of the mode A is centered at the anti-Stokes sideband ( $\Omega_A = \omega_m$ ) and the output of mode B is centered at the Stokes sideband ( $\Omega_B = -\omega_m$ ), for two different values of  $\epsilon$ .

i.e., larger input powers. Here, the oscillating mirror induces Stokes and anti-Stokes sidebands for *both* driving lasers and therefore it may be nontrivial to establish which are the most-entangled output modes. Fig. 11(a) shows that the largest all-optical entanglement is achieved between the *anti-Stokes sideband of the “cooling” mode and the Stokes sideband of the “heating” beam*. This is consistent with the results for a single cavity mode, because in both cases the motion of the resonator creates strong quantum correlations between the scattering of a Stokes and an anti-Stokes photon. Moreover this result can be understood from the fact that the two sidebands are those which are resonant with the corresponding cavity mode. Fig. 11(a) also shows that, as it happens in the single cavity mode case, and differently from the optomechanical entanglement, the all-optical  $E_{\mathcal{N}}$  monotonically increases for decreasing detection bandwidths. This is reasonable because the two output modes are correlated as in two-mode squeezing which is based on the pairwise correlated production of photons from a pump laser beam via a parametric process. In this case the quantum correlations are optimally detected when only pairs of photons exactly satisfying the matching condition  $\omega_s + \omega_{as} = \omega_{0A} + \omega_{0B}$  are detected, i.e., when  $\tau = \infty$ .

Fig. 11(b) instead shows the robustness of all-optical entanglement with respect to the reservoir temperature, which is extremely good: entanglement persists even at room temperature provided that one considers output modes with a sufficiently narrow bandwidth. In this respect, the bichromatic driving case proves to be more promising than the single driving mode case (compare Fig. 11(b) with Fig. 8(c)).

Combining all the results of this section, we see that the output modes associated with the two driven cavity modes and the mechanical mode form a tripartite system in which each bipartite subsystem is entangled. This suggests that a parameter region exists where this tripartite system is characterized by a fully tripartite-entangled stationary state. This is actually true and it can be checked by applying the classification criterion of Ref. [97], providing a necessary and sufficient criterion for the determination of the entanglement class in the case of tripartite CV Gaussian states, which is directly computable in terms of the eigenvalues of appropriate test matrices [97].

## 6 Cavity-mediated atom-mirror stationary entanglement

A final recent application of optomechanical systems, recently suggested by a number of papers (see Refs. [70,71]), is to couple them also to atomic ensembles in order to realize new and more flexible CV quantum interfaces. To be more specific, here we consider a hybrid system comprised of  $N_a$  two-level atoms of energy splitting  $\hbar\omega_a$ , coupled to an optical cavity, which is in turn coupled to a mechanical element by radiation pressure. We consider again the steady state of the system and choose a weak-coupling regime where the atoms and the cavity are far-off resonance (as illustrated by Fig. 12). The working point for the optomechanical system is the regime described in the previous section where red-detuned driving of the cavity ensures optimal entanglement between the Stokes sideband and the mechanical resonator. We show here that when the atoms are resonant with the Stokes sideband of the laser, a regime where both atoms-mirror bipartite CV entanglement and tripartite CV entanglement can be generated in the steady state, is achieved.

We start from the Hamiltonian of Eq. (1) to which we add the Tavis-Cummings atom-cavity field interaction

$$H_I = \hbar g (S_+ a + S_- a^\dagger),$$

where collective spin operators are defined as  $S_{+,-,z} = \sum_{\{i\}} \sigma_{+,-,z}^{(i)}$  for  $i = 1, N_a$  ( $\sigma_{+,-,z}$  are the Pauli matrices) and satisfy the commutation relations  $[S_+, S_-] = S_z$  and  $[S_z, S_\pm] = \pm 2S_\pm$ . The atom-cavity coupling constant is given by  $g = \mu \sqrt{\omega_c / 2\hbar\epsilon_0 V}$  where  $V$  is the cavity mode volume,  $\mu$  is the dipole moment of the atomic transition, and  $\epsilon_0$  is the free space permittivity.

The dynamics of the tripartite system is fairly complicated. However, one can find a regime where a simpler dynamics of three coupled harmonic oscillators is a good approximation of the system dynamics. To this purpose, we assume that the atoms are initially prepared in their ground state, so that  $S_z \simeq \langle S_z \rangle \simeq -N_a$  and this condition is not appreciably altered by the interaction

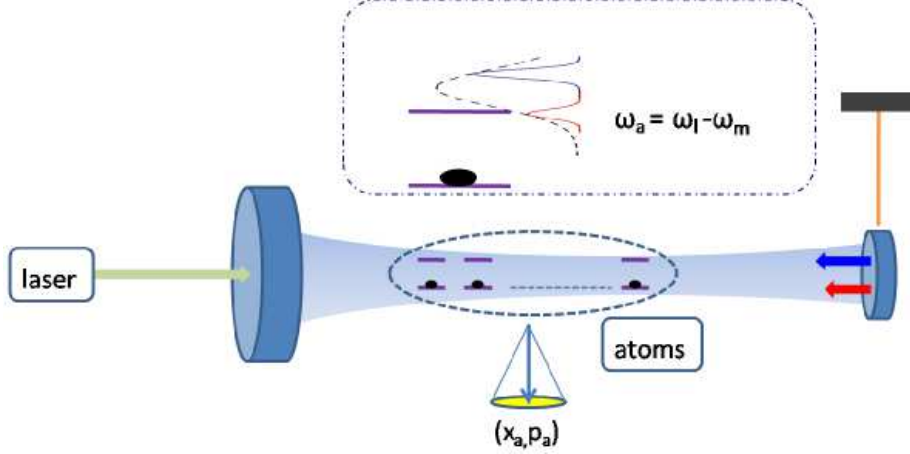


Fig. 12. Setup for tripartite hybrid entanglement. An atomic cloud of two-level atoms is placed inside a cavity driven by a laser. As seen in the inset, the atoms are resonant with the Stokes sideband of the laser. Since this latter sideband is the one carrying most of the optomechanical entanglement, also the atoms and movable mirror become entangled at the steady state.

with the cavity field. This is satisfied when the excitation probability of a single atom is small. In this limit the dynamics of the atomic polarization can be described in terms of bosonic operators: in fact if one defines the atomic annihilation operator  $c = S_- / \sqrt{|\langle S_z \rangle|}$ , one can see that it satisfies the usual bosonic commutation relation  $[c, c^\dagger] = 1$  [98]. In the frame rotating at the laser frequency  $\omega_l$  for the atom-cavity system, the quantum Langevin equations can then be written as

$$\dot{q} = \omega_m p, \quad (92)$$

$$\dot{p} = -\omega_m q - \gamma_m p + G_0 a^\dagger a + \xi, \quad (93)$$

$$\dot{a} = -(\kappa + i\Delta_0)a + iG_0 a q - iG_a c + \mathcal{E}_l + \sqrt{2\kappa} a_{in}, \quad (94)$$

$$\dot{c} = -(\gamma_a + i\Delta_a)c - iG_a a + \sqrt{2\gamma_a} F_c, \quad (95)$$

where  $\Delta_0 = \omega_c - \omega_l$  and  $\Delta_a = \omega_a - \omega_l$  are the cavity and atomic detuning with respect to the laser,  $G_a = g\sqrt{N_a}$ , and  $2\gamma_a$  is the decay rate of the atomic excited level. The noise affecting the atoms has one non-vanishing correlation function  $\langle F_c(t) F_c^\dagger(t') \rangle = \delta(t - t')$ . We now assume that the cavity is intensely driven, so that at the steady state, the intracavity field has a large amplitude  $\alpha_s$ , with  $|\alpha_s| \gg 1$ . However, the single-atom excitation probability is  $g^2|\alpha_s|^2/(\Delta_a^2 + \gamma_a^2)$  and since this probability has to be much smaller than one for the validity of the bosonic description of the atomic polarization, this imposes an upper bound to  $|\alpha_s|$ . Therefore the two conditions are simultaneously satisfied only if the atoms are weakly coupled to the cavity,  $g^2/[\Delta_a^2 + \gamma_a^2] \ll |\alpha_s|^{-2} \ll 1$ .

If one is interested only in atoms-mirror entanglement, one could assume a bad cavity limit and adiabatically eliminate the cavity mode [71]. However, one

can have a more complete information by linearizing the Langevin equations Eqs. (92)-(95) around the semiclassical steady state and then solving for the exact solution of the 3-mode system steady state provided by the Lyapunov equation (29) [70]. In fact, owing to the Gaussian nature of the quantum noise terms  $\xi$ ,  $a_{in}$  and  $F_c$ , and to the linearization of the dynamics, the steady state of the quantum fluctuations of the system is a CV tripartite Gaussian state, which is completely determined by its  $6 \times 6$  correlation matrix (CM). The corresponding drift matrix after linearization is given by

$$A = \begin{pmatrix} 0 & \omega_m & 0 & 0 & 0 & 0 \\ -\omega_m & -\gamma_m & G & 0 & 0 & 0 \\ 0 & 0 & -\kappa & \Delta & 0 & G_a \\ G & 0 & -\Delta & -\kappa & -G_a & 0 \\ 0 & 0 & 0 & G_a & -\gamma_a & \Delta_a \\ 0 & 0 & -G_a & 0 & -\Delta_a & -\gamma_a \end{pmatrix}, \quad (96)$$

while the diffusion matrix is equal to  $D = \text{diag}[0, \gamma_m(2n_0 + 1), \kappa, \kappa, \gamma_a, \gamma_a]$ . We have solved Eq. (29) for the CM  $\mathcal{V}$  in a wide range of the parameters  $G$ ,  $G_a$ ,  $\Delta$  and  $\Delta_a$ . We have studied first of all the stationary entanglement of the three possible bipartite subsystems, by quantifying it in terms of the logarithmic negativity of bimodal Gaussian states. We will denote the logarithmic negativities for the mirror-atom, atom-field and mirror-field bimodal partitions with  $E_{ma}$ ,  $E_{af}$  and  $E_{mf}$ , respectively.

The results on the behavior of the bipartite entanglement  $E_{ma}$  are shown in Fig. 13a. Optimization requires, as expected that the atoms are resonant with the Stokes motional sideband. In Fig. 13b, the logarithmic negativity of the three bipartitions is plotted versus the normalized atomic detuning. It is evident that one has a sort of entanglement sharing: due to the presence of the atoms, the initial cavity-mirror entanglement (represented by the dashed line) is partially redistributed to the atom-mirror and atom-cavity subsystems and this effect is predominant when the atoms are resonant with the Stokes sideband ( $\Delta_a = -\omega_m$ ). It is remarkable that, in the chosen parameter regime, the largest stationary entanglement is the one between atoms and mirror which are only indirectly coupled. Moreover, the nonzero atom-cavity entanglement appears only thanks to the effect of the mirror dynamics because in the bosonic approximation we are considering and with a fixed mirror, there would be no direct atom-cavity entanglement. We also notice that atom-mirror entanglement is instead not present at  $\Delta_a = \omega_m$ . This is due to the fact that the cavity-mirror entanglement is mostly carried by the Stokes sideband and that, when  $\Delta_a = \omega_m$ , mirror cavity-cooling is disturbed by the anti-Stokes photons being recycled in the cavity by the absorbing atoms.



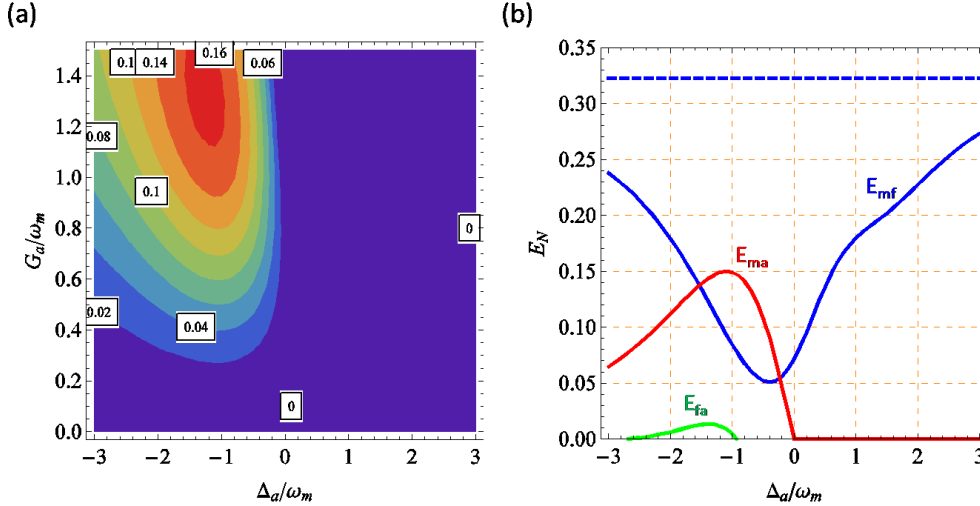


Fig. 13. Entanglement in the hybrid mirror-atom-field system. Parameters are  $p_0$ ,  $\kappa = \gamma_a = \omega_m$ ,  $G = 1.3\omega_m$ . (a) Contour plot of  $E_{\mathcal{N}}$  between mirror and atoms as a function of  $G_a/\omega_m$  and  $\Delta_a/\omega_m$ . The entanglement is optimized for  $\Delta_a = -\omega_m$ , i.e. when the atoms are resonant with the Stokes sideband of the laser. (b) The three bipartite entanglement versus the atomic detuning. The blue dashed line represents the mirror-field  $E_{\mathcal{N}}$  in the absence of atom-field coupling. When the atoms are immersed in the mirror-field system, the entanglement is redistributed among the three sub-partitions, especially around the regime where  $\Delta_a = -\omega_m$ .

We notice that the chosen parameters correspond to a small cavity mode volume ( $V \simeq 10^{-12} \text{ m}^3$ ), implying that for a dipole transition,  $g$  is not small. Therefore the assumed weak coupling condition  $g^2/[\Delta_a^2 + \gamma_a^2] \ll |\alpha_s|^{-2} \ll 1$  can be satisfied only if  $g$  represents a much smaller, *time averaged*, coupling constant. This holds for example for an atomic vapor cell much larger than the cavity mode: if the (hot) atoms move in a cylindrical cell with axis orthogonal to the cavity axis, with diameter  $\sim 0.5 \text{ mm}$  and height  $\sim 1 \text{ cm}$ , they will roughly spend only one thousandth of their time within the cavity mode region. This yields an effective  $g \sim 10^4 \text{ Hz}$ , so that the assumptions made here hold, and the chosen value  $G_a/2\pi = 6 \times 10^6 \text{ Hz}$  can be obtained with  $N_a \sim 10^7$ . An alternative solution could be choosing a cold atomic ensemble and a dipole-forbidden transition.

The entanglement properties of the steady state of the tripartite system can be verified by experimentally measuring the corresponding CM. This can be done by combining existing experimental techniques. The cavity field quadratures can be measured directly by homodyning the cavity output, while the mechanical position and momentum can be measured with the schemes discussed in Sec. 3.3. Finally, the atomic polarization quadratures  $x$  and  $y$  (proportional to  $S_x$  and  $S_y$ ) can be measured by adopting the same scheme of Ref. [99], i.e., by making a Stokes parameter measurement of a laser beam, shined transversal to the cavity and to the cell and off-resonantly tuned to another atomic transition.

## 7 Conclusions

The search for experimental demonstrations of the quantum behavior of macroscopic mechanical resonators is a fastly growing field of investigation. Recent experimental results [15,16,17,18,19,20,21,22,23,24,25,26,27,28,29,30,31] and theoretical predictions suggest that quantum states of resonators with a mass at the microgram scale will be generated and detected in the near future. In this chapter we have tried to give an overview of two relevant arguments of this research field: i) cooling to the motional ground state; ii) the generation of robust entangled steady states involving mechanical and optical degrees of freedom. The latter condition is the fundamental prerequisite for the eventual integration of micro- and nano-mechanical resonators serving as quantum memories and interfaces within quantum communication networks.

In the first part of the chapter we have described and compared the two main approaches for cooling micro-mechanical resonators via radiation pressure coupling to an optical cavity, cold-damping feedback [32,34,35,36,41], and back-action cooling [33,39,40,41,42,43]. We have adopted a general quantum Langevin treatment which is valid within the full parameter range of a stable cavity. Both back-action cooling and cold damping feedback are able to cool to the ground state, even though back-action cooling is preferable for a good cavity ( $\kappa < \omega_m$ ), while cold damping is more convenient for a bad cavity ( $\kappa > \omega_m$ ).

In the second part of the chapter we have analyzed the entanglement properties of the steady state of the system formed by the optical cavity coupled to a mechanical element. We have considered two different configurations, with either one or two intensely driven cavity modes. We have seen that the intracavity mode and the mechanical element can be entangled in a robust way against temperature, and that back-action cooling is *not* a necessary condition for achieving entanglement. In fact, entanglement is possible also in the opposite regime of a blue-detuned laser where the cavity mode *drives* and does not cool the resonator. More generally, the two phenomena are quite independent, and one is not necessarily accompanied by the other. Cooling is a classical process (even though it can ultimately lead to the quantum ground state), while entanglement is an intrinsically quantum phenomenon. Moreover, they are optimized in different parameter regimes. In fact, logarithmic negativity is maximized close to the stability threshold of the system, where instead the resonator is not cooled. We have then focused our study onto the entanglement properties of the cavity output field, which is the relevant one for quantum communication applications. We have developed a general theory showing how it is possible to define and evaluate the entanglement properties of the multipartite system formed by the mechanical resonator and  $N$  independent output modes of the cavity field. We have seen that the tripartite

system formed by the mechanical element and the two output modes centered at the first Stokes and anti-Stokes sideband of the driving laser (where the cavity output noise spectrum is concentrated) shows robust fully tripartite entanglement. In particular, the Stokes output mode is strongly entangled with the mechanical mode and shows a sort of entanglement distillation because its logarithmic negativity is significantly larger than the intracavity one when its bandwidth is appropriately chosen. In the same parameter regime, the Stokes and anti-Stokes sideband modes are robustly entangled, and the achievable entanglement in the limit of a very narrow detection bandwidth is comparable to that generated by a parametric oscillators. These results hold in both cases of single and bichromatic driving of the cavity. In this latter case, entanglement becomes larger and more robust against temperature under a particular parameter condition in which one mode is driven by a red-detuned laser and the other one by a blue-detuned laser. In fact, for equal optomechanical couplings and opposite detunings the system is always stable, even for large values of the intracavity power, and entanglement can persist also at higher temperatures.

Finally we have investigated a possible route for coupling optomechanical devices with atomic ensembles, by showing that if the atoms are placed inside the optical cavity and tuned into resonance with the Stokes sideband, optomechanical entanglement is optimally distributed also to the atomic ensemble [70]. Under these conditions one realizes a strongly coupled system showing robust tripartite entanglement which can be exploited for the realization of CV quantum interfaces [71].

## 8 Acknowledgements

This work has been supported by the European Commission (FP6 Integrated Project QAP, and FET-Open project MINOS), and by INFN (SQUALO project).

## References

- [1] M. P. Blencowe, *Phys. Rep.* **395**, 159 (2004).
- [2] K. C. Schwab and M. L. Roukes, *Phys. Today* **58**, 36 (2005).
- [3] T. J. Kippenberg and K. J. Vahala, *Opt. Expr.* **15**, 17172 (2007).
- [4] M. Aspelmeyer and K. Schwab, *New J. Phys.* **10** 095001 (2008).

- [5] V.B. Braginsky and F. Ya Khalili, *Quantum Measurements*, Cambridge University Press, Cambridge, (1992).
- [6] B. Abbott *et al.*, Phys. Rev. D **69**, 122004 (2004); F. Acernese *et al.* Class. Quantum Grav. **22** S869 (2005).
- [7] W. Marshall, C. Simon, R. Penrose, and D. Bouwmeester, Phys. Rev. Lett. **91**, 130401 (2003). W. H. Zurek, Rev. Mod. Phys. **75**, 715 (2003).
- [8] A. J. Leggett, J. Phys. Cond. Mat., **14**, R415 (2002).
- [9] L. Hackermüller, K. Hornberger, B. Brezger, A. Zeilinger, and M. Arndt, Nature (London) **427**, 711 (2004).
- [10] B. Julsgaard, A. Kozhekin, E. S. Polzik, Nature (London) **413**, 400 (2001).
- [11] A. J. Berkley, H. Xu, R. C. Ramos, M. A. Gubrud, F. W. Strauch, P. R. Johnson, J. R. Anderson, A. J. Dragt, C. J. Lobb, F. C. Wellstood, Science **300**, 1548 (2003).
- [12] P. F. Cohadon, A. Heidmann, and M. Pinard, Phys. Rev. Lett. **83**, 3174 (1999).
- [13] M. D. LaHaye, O. Buu, B. Camarota, and K. C. Schwab, Science **304**, 74 (2004).
- [14] C. H. Metzger and K. Karrai, Nature (London), **432**, 1002 (2004).
- [15] A. Naik, O. Buu, M. D. LaHaye, A. D. Armour, A. A. Clerk, M. P. Blencowe, and K. C. Schwab, Nature **443**, 193 (2006).
- [16] O. Arcizet, P.-F. Cohadon, T. Briant, M. Pinard, and A. Heidmann, J. M. Mackowski, C. Michel, L. Pinard, O. Francais, L. Rousseau, Phys. Rev. Lett. **97**, 133601 (2006).
- [17] S. Gigan, H. Böhm, M. Paternostro, F. Blaser, G. Langer, J. Hertzberg, K. Schwab, D. Bäuerle, M. Aspelmeyer, and A. Zeilinger, Nature (London) **444**, 67 (2006).
- [18] O. Arcizet, P.-F. Cohadon, T. Briant, M. Pinard, and A. Heidmann, Nature (London) **444**, 71 (2006).
- [19] D. Kleckner and D. Bouwmeester, Nature (London) **444**, 75 (2006).
- [20] A. Schliesser, P. Del’Haye, N. Nooshi, K. J. Vahala, and T. J. Kippenberg, Phys. Rev. Lett. **97** 243905 (2006).
- [21] T. Corbitt, Y. Chen, E. Innerhofer, H. Müller-Ebhardt, D. Ottaway, H. Rehbein, D. Sigg, S. Whitcomb, C. Wipf, and N. Mavalvala, Phys. Rev. Lett. **98**, 150802 (2007); T. Corbitt, C. Wipf, T. Bodiya, D. Ottaway, D. Sigg, N. Smith, S. Whitcomb, and N. Mavalvala, Phys. Rev. Lett. **99**, 160801 (2007).
- [22] M. Poggio, C. L. Degen, H. J. Mamin, and D. Rugar, Phys. Rev. Lett. **99**, 017201 (2007).
- [23] K. R. Brown, J. Britton, R. J. Epstein, J. Chiaverini, D. Leibfried, and D. J. Wineland, Phys. Rev. Lett. **99**, 137205 (2007).

- [24] S. Groblacher, S. Gigan, H. R. Boehm, A. Zeilinger, M. Aspelmeyer, *Europhys. Lett.* **81**, 54003 (2008).
- [25] A. Schliesser, R. Rivière, G. Anetsberger, O. Arcizet, and T. J. Kippenberg, *Nat. Phys.* **4**, 415 (2008).
- [26] J. D. Thompson, B. M. Zwickl, A. M. Jayich, F. Marquardt, S. M. Girvin, and J. G. E. Harris, *Nature (London)* **452**, 72 (2008).
- [27] C. A. Regal, J. D. Teufel, K. W. Lehnert, *Nat. Phys.* **4**, 555 (2008).
- [28] A. Vinante *et al.*, *Phys. Rev. Lett.* **101**, 033601 (2008).
- [29] J. D. Teufel, J. W. Harlow, C. A. Regal, and K. W. Lehnert, *Phys. Rev. Lett.* **101**, 197203 (2008).
- [30] A. Schliesser, O. Arcizet, R. Rivière, T. J. Kippenberg, arXiv:0901.1456v1 [quant-ph].
- [31] S. Groblacher, J. B. Hertzberg, M. R. Vanner, S. Gigan, K. C. Schwab, M. Aspelmeyer, arXiv:0901.1801v1 [quant-ph].
- [32] S. Mancini, D. Vitali, and P. Tombesi, *Phys. Rev. Lett.* **80**, 688 (1998).
- [33] V. B. Braginsky, S. E. Strigin, and S. P. Vyatchanin, *Phys. Lett. A* **287**, 331 (2001).
- [34] J.-M. Courty, A. Heidmann, and M. Pinard, *Eur. Phys. J. D* **17**, 399 (2001).
- [35] D. Vitali, S. Mancini, and P. Tombesi, *Phys. Rev. A* **64**, 051401(R) (2001).
- [36] D. Vitali, S. Mancini, L. Ribichini, and P. Tombesi, *Phys. Rev. A* **65** 063803 (2002); **69**, 029901(E) (2004); *J. Opt. Soc. Am. B* **20**, 1054 (2003).
- [37] I. Wilson-Rae, P. Zoller, and A. Imamoglu, *Phys. Rev. Lett.* **92**, 075507 (2004).
- [38] I. Martin, A. Shnirman, L. Tian, and P. Zoller, *Phys. Rev. B* **69**, 125339 (2004)
- [39] F. Marquardt, J. P. Chen, A. A. Clerk, and S. M. Girvin, *Phys. Rev. Lett.* **99**, 093902 (2007).
- [40] I. Wilson-Rae, N. Nooshi, W. Zwerger, and T. J. Kippenberg, *Phys. Rev. Lett.* **99**, 093901 (2007).
- [41] C. Genes, D. Vitali, P. Tombesi, S. Gigan, and M. Aspelmeyer, *Phys. Rev. A* **77**, 033804 (2008).
- [42] A. Dantan, C. Genes, D. Vitali, and M. Pinard, *Phys. Rev. A* **77**, 011804(R) (2008).
- [43] J. M. Dobrindt, I. Wilson-Rae, and T. J. Kippenberg, *Phys. Rev. Lett.* **101**, 263602 (2008).
- [44] K. W. Murch, K. L. Moore, S. Gupta, and D. M. Stamper-Kurn, *Nature Phys.* **4**, 561 (2008); F. Brennecke, S. Ritter, T. Donner, T. Esslinger, *Science* **322**, 235 (2008).

- [45] M. P. Blencowe and M. N. Wybourne, *Physica B* **280**, 555 (2000).
- [46] P. Rabl, A. Shnirman and P. Zoller, *Phys. Rev. B* **70**, 205304 (2004); X. Zhou and A. Mizel, *Phys. Rev. Lett.* **97**, 267201 (2006); K. Jacobs, *Phys. Rev. Lett.* **99**, 117203 (2007); W. Y. Huo, G. L. Long, *Appl. Phys. Lett.* **92**, 133102 (2008).
- [47] R. Ruskov, K. Schwab and A. N. Korotkov, *Phys. Rev. B* **71**, 235407 (2005); A. A. Clerk, F. Marquardt and K. Jacobs, *New J. Phys.* **10**, 095010 (2008); M. J. Woolley, A. C. Doherty, G. J. Milburn, K. C. Schwab, *Phys. Rev. A* **78**, 062303 (2008).
- [48] J. S. Bell, *Physics (N.Y.)* **1**, 195 (1964).
- [49] S. Mancini, V. Giovannetti, D. Vitali and P. Tombesi, *Phys. Rev. Lett.* **88**, 120401 (2002).
- [50] A. D. Armour, M. P. Blencowe, K. C. Schwab, *Phys. Rev. Lett.* **88**, 148301 (2002).
- [51] J. Eisert, M. B. Plenio, S. Bose, J. Hartley, *Phys. Rev. Lett.* **93**, 190402 (2004).
- [52] X. Zou and W. Mathis, *Phys. Lett. A* **324**, 484-488 (2004).
- [53] A. N. Cleland and M. R. Geller, *Phys. Rev. Lett.* **93**, 070501 (2004).
- [54] L. Tian and P. Zoller, *Phys. Rev. Lett.* **93**, 266403 (2004).
- [55] L. Tian, *Phys. Rev. B* **72**, 195411 (2005).
- [56] F. Xue, Y. X. Liu, C. P. Sun, and F. Nori, *Phys. Rev. B* **76**, 064305 (2007).
- [57] A. K. Ringsmuth and G. J. Milburn, *J. Mod. Opt.* **54** 2223 (2007).
- [58] D. Vitali, P. Tombesi, M. J. Woolley, A. C. Doherty, G. J. Milburn, *Phys. Rev. A* **76**, 042336 (2007).
- [59] J. Zhang, K. Peng, and S. L. Braunstein, *Phys. Rev. A* **68**, 013808 (2003).
- [60] M. Pinard, A. Dantan, D. Vitali, O. Arcizet, T. Briant, A. Heidmann, *Europhys. Lett.* **72**, 747 (2005).
- [61] M. Paternostro, D. Vitali, S. Gigan, M. S. Kim, C. Brukner, J. Eisert, and M. Aspelmeyer, *Phys. Rev. Lett.* **99**, 250401 (2007).
- [62] M. Bhattacharya and P. Meystre, *Phys. Rev. Lett.* **99**, 073601 (2007); *Phys. Rev. Lett.* **99**, 153603 (2007); M. Bhattacharya, H. Uys, and P. Meystre, *Phys. Rev. A* **77**, 033819 (2008).
- [63] C. Wipf, T. Corbitt, Y. Chen, N. Mavalvala, *New J. Phys.* **10**, 095017 (2008).
- [64] D. Vitali, S. Gigan, A. Ferreira, H. R. Böhm, P. Tombesi, A. Guerreiro, V. Vedral, A. Zeilinger, and M. Aspelmeyer, *Phys. Rev. Lett.* **98**, 030405 (2007).
- [65] D. Vitali, S. Mancini, and P. Tombesi, *J. Phys. A: Math. Theor.* **40**, 8055 (2007).

- [66] S. Mancini, D. Vitali, and P. Tombesi, Phys. Rev. Lett. **90**, 137901 (2003); S. Pirandola, S. Mancini, D. Vitali, and P. Tombesi, Phys. Rev. A **68**, 062317 (2003).
- [67] S. Pirandola S. Mancini, D. Vitali, and P. Tombesi, J. Mod. Opt. **51**, 901 (2004).
- [68] S. Pirandola, D. Vitali, P. Tombesi, and S. Lloyd, Phys. Rev. Lett. **97**, 150403 (2006).
- [69] C. Genes, A. Mari, P. Tombesi, and D. Vitali, Phys. Rev. A **78**, 032316 (2008).
- [70] C. Genes, D. Vitali, and P. Tombesi, Phys. Rev. A **77**, 050307(R) (2008).
- [71] H. Ian, Z. R. Gong, Yu-xi Liu, C. P. Sun, and F. Nori, Phys. Rev. A **78**, 013824 (2008); K. Hammerer, M. Aspelmeyer, E. S. Polzik, and P. Zoller, Phys. Rev. Lett. **102**, 020501 (2009).
- [72] T. J. Kippenberg, H. Rokhsari, T. Carmon, A. Scherer, and K. J. Vahala,, Phys. Rev. Lett. **95** 033901 (2005).
- [73] M. Pinard, Y. Hadjar, and A. Heidmann, Eur. Phys. J. D **7**, 107 (1999).
- [74] C. Genes, D. Vitali, and P. Tombesi, New J. Phys. **10**, 095009 (2008).
- [75] V. Giovannetti, D. Vitali, Phys. Rev. A **63**, 023812 (2001).
- [76] C. K. Law, Phys. Rev. A **51**, 2537 (1995).
- [77] L. Landau, E. Lifshitz, *Statistical Physics* (Pergamon, New York, 1958).
- [78] R. Benguria, and M. Kac, Phys. Rev. Lett, **46**, 1 (1981).
- [79] C. W. Gardiner and P. Zoller, *Quantum Noise*, (Springer, Berlin, 2000).
- [80] S. Mancini and P. Tombesi, Phys. Rev. A **49**, 4055 (1994).
- [81] I. S. Gradshteyn and I. M. Ryzhik, *Table of Integrals, Series and Products*, Academic Press, Orlando, 1980, pag. 1119.
- [82] F. Marquardt, J. G. Harris, and S. M. Girvin , Phys. Rev. Lett. **96**, 103901 (2006).
- [83] A. Dorsel, J.D. McCullen, P. Meystre, E. Vignes, and H. Walther, Phys. Rev. Lett. **51**, 1550 (1983); A. Gozzini, F. Maccarone, F. Mango, I. Longo, and S. Barbarino, J. Opt. Soc. Am. B **2**, 1841 (1985).
- [84] J. Eisert, Ph.D. thesis, University of Potsdam, 2001; G. Vidal and R. F. Werner, Phys. Rev. A **65**, 032314 (2002); G. Adesso *et al.*, Phys. Rev. A **70**, 022318 (2004).
- [85] R. Simon, Phys. Rev. Lett. **84**, 2726 (2000).
- [86] M. M. Wolf, G. Giedke and J. I. Cirac, Phys. Rev. Lett. **96**, 080502 (2006).
- [87] S. Stenholm, Rev. Mod. Phys. **58**, 699 (1986).

- [88] D. Leibfried, R. Blatt, C. Monroe, and D. Wineland, *Rev. Mod. Phys.* **75**, 281 (2003).
- [89] G.M. DAriano, M. G. A. Paris, M. F. Sacchi, *Adv. Imag. Electr. Phys.* **128**, 205 (2003).
- [90] C. W. Gardiner and P. Zoller, *Quantum Noise*, (Springer, Berlin, 2000), p. 71.
- [91] M. S. Kim, W. Son, V. Bužek, and P. L. Knight, *Phys. Rev. A* **65**, 032323 (2002).
- [92] S. J. van Enk and C. A. Fuchs, *Phys. Rev. Lett.* **88**, 027902 (2002); D. Vitali, P. Canizares, J. Eschner, and G. Morigi, *New J. Phys.* **10**, 033025 (2008).
- [93] V. Giovannetti, S. Mancini, and P. Tombesi, *Europhys. Lett.* **54**, 559 (2001).
- [94] S. Giannini, S. Mancini, and P. Tombesi, *Quant. Inf. Comp.* **3**, 265-279 (2003).
- [95] S. Pirandola, S. Mancini, D. Vitali, P. Tombesi, *J. Opt. B: Quantum Semiclass. Opt.* **5**, S523-S529 (2003).
- [96] G. Morigi, J. Eschner, S. Mancini, and D. Vitali, *Phys. Rev. Lett.* **96**, 023601 (2006); *Phys. Rev. A* **73**, 033822 (2006); D. Vitali, G. Morigi, and J. Eschner, *Phys. Rev. A* **74**, 053814 (2006).
- [97] G. Giedke, B. Kraus, M. Lewenstein, and J. I. Cirac, *Phys. Rev. A* **64**, 052303 (2001).
- [98] T. Holstein, and H. Primakoff, *Phys. Rev.* **58**, 1098 (1940).
- [99] J. Sherson, H. Krauter, R. K. Olsson, B. Julsgaard, K. Hammerer, I. Cirac, E. S. Polzik, *Nature* **443**, 557 (2006).